JCI insight

Durable Hematopoiesis and Tolerance After Vertebral Bone Marrow Transplant from a Deceased Lung Transplant Donor

Paul Szabolcs, Xiaohua Chen, Marian G. Michaels, Memphis Hill, Evelyn Garchar, Zarreen Amin, Heather M. Stanczak, Shawna McIntyre, Aleksandra Petrovic, Dhivyaa Rajasundaram, Ansuman Chattopadhyay, Jonathan E. Spahr, Peter D. Wearden, Geoffrey Kurland

JCI Insight. 2026. https://doi.org/10.1172/jci.insight.198029.

Research In-Press Preview **Clinical Research** **Hematology** **Immunology**

We hypothesized that performing bone marrow transplant (BMT) using marrow extracted from the vertebral bodies (VB) of an unrelated deceased lung transplant (LTX) donor would be able to establish persistent hematopoiesis, generate immunity, and tolerance. A teenager with severe combined immunodeficiency with lung failure due to recurrent pneumonias underwent LTX in 2016 from a 1/8 HLA allele-matched unrelated donor, followed by BMT 4 months later using T-cell/B-cell-depleted, cryopreserved VB marrow. Rapid engraftment was followed by accelerating immune competence at 6 months, with independence from immunosuppression by 16 months. Donor T-cell (>95%) and myeloid chimerism (7-10%) have persisted for over nine years. At two years post-BMT, circulating T cells were hyporesponsive to host dendritic cells *in vitro*. T-cell receptor clonotyping revealed the disappearance of host-reactive clones, and T-cell RNA-sequencing exhibited downmodulated signaling pathways for cytotoxicity/rejection, paired with upregulated immunomodulatory pathways, suggesting active suppression. In parallel, host monocytes upregulated certain signaling pathways, indicating active interactions between post-thymic donor T cells and host monocytes. In summary, durable hematopoietic engraftment, immunity, and tolerance were demonstrable for the first time in a recipient of BMT obtained from VB graft.

Durable Hematopoiesis and Tolerance After Vertebral Bone Marrow Transplant from a Deceased Lung Transplant Donor

Paul Szabolcs[*,1,2], Xiaohua Chen[1], Marian G. Michaels[3], Memphis Hill[1], Evelyn Garchar[1], Zarreen Amin[1], Heather M Stanczak[1,4], Shawna McIntyre[1], Aleksandra Petrovic[5], Dhivyaa Rajasundaram[6], Ansuman Chattopadhyay[7], Jonathan E Spahr[8], Peter D Wearden[9], and Geoffrey Kurland[8]

[1]*Division of Blood and Marrow Transplantation and Cellular Therapy, UPMC Children's Hospital of Pittsburgh*
[2]*Department of Immunology, University of Pittsburgh*
[3]*Division of Infectious Diseases, UPMC Children's Hospital of Pittsburgh, University of Pittsburg*
[4]*Hematopoietic Stem Cell Laboratories, UPMC Children's Hospital of Pittsburgh*
[5]*Department of Pediatrics, University of Washington- Seattle Children's Hospital, Seattle, WA*
[6]*Division of Health Informatics, UPMC Children's Hospital of Pittsburgh, University of Pittsburgh*
[7]*Molecular Biology Information Service, Health Sciences Library System, University of Pittsburgh*
[8]*Division of Pulmonary Medicine, Allergy & Immunology, UPMC Children's Hospital of Pittsburgh, University of Pittsburgh*
[9]*Department of Cardiovascular Services, Nemours Children's Hospital, Orlando, FL*

Running Title: Deceased donor vertebral marrow transplantation

Disclosure of Conflict of Interest: The authors have declared that no conflict of interest exists.

*Corresponding author:
Paul Szabolcs, MD
Division of Blood and Marrow Transplantation and Cellular Therapy
UPMC Children's Hospital of Pittsburgh
4401 Penn Ave, Rangos Bldg. 5125, Pittsburgh, PA, 15224
Phone: 412-692-6225
Email: paul.szabolcs@chp.edu

Abstract

We hypothesized that performing bone marrow transplant (BMT) using marrow extracted from the vertebral bodies (VB) of an unrelated deceased lung transplant (LTX) donor would be able to establish persistent hematopoiesis, generate immunity, and tolerance. A teenager with severe combined immunodeficiency with lung failure due to recurrent pneumonias underwent LTX in 2016 from a 1/8 HLA allele-matched unrelated donor, followed by BMT 4 months later using T-cell/B-cell-depleted, cryopreserved VB marrow. Rapid engraftment was followed by accelerating immune competence at 6 months, with independence from immunosuppression by 16 months. Donor T-cell (>95%) and myeloid chimerism (7-10%) have persisted for over nine years. At two years post-BMT, circulating T cells were hyporesponsive to host dendritic cells *in vitro*. T-cell receptor clonotyping revealed the disappearance of host-reactive clones, and T-cell RNA-sequencing exhibited downmodulated signaling pathways for cytotoxicity/rejection, paired with upregulated immunomodulatory pathways, suggesting active suppression. In parallel, host monocytes upregulated certain signaling pathways, indicating active interactions between post-thymic donor T cells and host monocytes. In summary, durable hematopoietic engraftment, immunity, and tolerance were demonstrable for the first time in a recipient of BMT obtained from VB graft.

Trial registration: Pitt IRB Pro:13040207, FDA-IND:15414

Funding: UPMC Children's Hospital 'Start Up' fund #25510

Introduction

Patients with primary immunodeficiency (PID) syndromes are prone to developing progressive pulmonary complications, such as bronchiectasis or interstitial lung disease (ILD) (1, 2). Recurrent pneumonias caused by Gram-positive and Gram-negative bacteria and *Aspergillus species* frequently occur, regardless of their PID genotypes (3). Bone marrow transplantation (BMT) or other forms of hematopoietic stem cell transplantation (HSCT) are the most common definitive therapies to prevent progression to pulmonary failure (2). By this time, most PID patients are no longer eligible for either bilateral orthotopic lung transplant (BOLT) or HSCT due to the futility of either intervention alone. Following BOLT and solid-organ transplants (SOT) in general, most patients require long-term immunosuppressive therapy (IST) to prevent rejection and graft loss. Despite IST, the five-year survival rate after BOLT remains limited to 55-60% primarily due to chronic lung allograft dysfunction (CLAD) as well as complications secondary to immunosuppression (4, 5) with susceptibility to infections, malignancies, and progressive organ and metabolic dysfunctions (6). Inducing donor-specific long-term immune tolerance could eliminate the need for prolonged IST. However, it is a realistic clinical endpoint after HSCT only with sustained engraftment of donor immune cells (7), as opposed to SOT performed alone, where long-term immune tolerance is rare, occurring primarily after liver allografts (8).

Donor-specific tolerance after performing HSCT from the same live kidney donor has been tested over the past 2-3 decades (9-15), with full donor or persistent mixed donor chimerism from matched unrelated or half-matched (≥4 of 8) related donors, providing the most likely successful platform (16-18). When BMT was performed for hematologic malignancies from sibling donors, IST-free kidney transplantation (KT) followed if the kidney was from the same sibling donor (19, 20). Strategies short of persistent donor 'macrochimerism' (>4%) have failed in the unrelated or HLA-mismatched donor setting. If all leukocytes are derived from the organ donor, tolerance may be relevant only in the context of graft-versus-host (GvH) direction, while bidirectional tolerance is required in cases of mixed donor-host T cell chimerism to overcome rejection (10, 11, 13).

Successful tolerance induction to a human lung allograft was previously reported only once by Szabolcs *et al*. using a cryopreserved CD3/CD19 cell-depleted marrow graft aspirated from the

iliac crest of an unrelated beating-heart donor, leading to full donor chimerism despite the patient receiving sub-myeloablative irradiation and chemotherapy (21).

Here we report what we believe to be the first human case of durable multilineage engraftment with vertebral bone marrow transplantation. The graft was recovered hours after cessation of circulation from the vertebral bodies of a deceased unrelated male lung allograft donor (Fig 1), and it provided protective cellular and humoral immunity for a decade despite matching at only a single HLA allele. IST-free survival without rejection or graft-versus-host disease (GvHD) established tolerance. The underlying mechanisms of long-term immune tolerance in the mixed-chimerism setting were also investigated in depth, demonstrating clonal deletion as a dominant, but not the sole mechanism responsible for IST independence.

Results

Engraftment of donor graft post-BMT

Following neutrophil engraftment at 2 weeks, 100% donor cell chimerism was documented at 1 month from whole blood sample, which was mostly comprised of myeloid cells (Fig 2B, 2D, Suppl Table 1). To overcome T-cell lymphopenia associated with the parallel emergence of host T cells (73% host at 2-months), the patient received donor leukocyte infusion (DLI) once containing ~5E+04 CD3+T cells/kg from a thawed, unmodified marrow aliquot. DLI resulted in rapid rise in donor T-cell contribution (99%), (Fig 2C, Suppl Table 1), paired with an increase in donor NK cells (93%) (Fig 1F, Suppl Table 1) in both peripheral blood (PB) and bronchoalveolar lavage (BAL). In contrast, the monocyte fraction was only 40% donor-derived (Fig 2D, Suppl Table 1). Donor T-cell chimerism above 95% (FC) has persisted throughout nine years (Fig 2C, Suppl Table 1), while donor contributions to monocytes, B cells, and NK cells have gradually declined until each stabilized ~2 years post-BMT and sustained beyond, (7-13%, 28-81%, and 2-7% respectively) (Fig 2D, 2E, 2F, Suppl Table 1). Serial BAL samples similarly exhibited mixed chimerism, with the last available sample tested at 18-month post-BMT showing 97% donor-derived T cells, 24% monocytes, 46% B cells, and 36% NK cells (Fig 2B-2F, Suppl Table 1).

Pulmonary status after BOLT and BMT

Pulmonary function tests with serial spirometry demonstrated rapid improvement after BOLT, with steady parameters pre- and post-IST withdrawal (Fig 2A) up to nearly 10 years since

BOLT. Transbronchial biopsies performed 3 times following BOLT and prior to BMT showed no acute cellular rejection (A0), no evidence of lymphocytic bronchiolitis (B0), and no evidence of chronic/airway rejection (C0). From 5 to 25 months following BOLT, only a single biopsy (15 months post-BOLT while still on Tacrolimus) showed A1 ("Minimal Acute Cellular rejection"), whereas all 3 subsequent and 7 prior lung biopsies reporting no evidence of rejection (A0, B0, C0) (data not shown).

Immune status before and after BMT

The patient's underlying IL-7 receptor (IL-7R) null severe combined immunodeficiency (SCID) was characterized by progressive T-cell lymphopenia pre-BOLT/pre-BMT (baseline) (Fig 3A, Suppl Table 2). T- and B-cell lymphopenia persisted in the early phase post-BMT, reflecting the use of a CD3/CD19 depleted graft combined with lympholytic serotherapy administered peri-transplant. DLI was administered on Day+68 for T-cell lymphopenia (CD3+T-cell N^{o}. <20/μL), resulting in a rapid increase in CD3+T-cell numbers by Day+90 post-BMT (CD3+:119/μL, CD4: 98/μL, CD8+: 19/μL), with minimal impact on CD4+FOXP3+Tregs (1.5/μL) and CD19+B-cells numbers (0.2/μL) (Fig 3A, Suppl Table 2). Very mild skin GvHD involving < 25% of body surface area appeared around 3-4 weeks post-DLI but cleared within two weeks after administration of oral prednisone (1mg/kg) with rapid taper plus topical therapy. Lymphopenia steadily improved over time (Fig 3A, Suppl Table 2). Nevertheless, naive CD4+T cells (CD3+CD4+CD45RA+CD62L+) remained almost undetectable (2/μL) until 6-months post-BMT (25/μL), at which point thymopoiesis accelerated. Thymic output reached near-peak levels around 18 months post-BMT and has remained stable - and even increased - at last evaluation (Fig 3A, Suppl Table 2).

Both signal joint T-cell receptor excision circles (sjTREC) copy numbers and T-cell receptor (TCR) spectratype complexity score (SCS) reached their nadir around day+30 post- BMT, reflecting profound T-cell depletion and use of a T-cell-depleted HSCT graft. These parameters returned to pre-BMT levels around 3-months (for TCRβ SCS) and 6-months (for sjTREC), with continued acceleration peaking around 2-years post-BMT (Fig 3B, 3C, Suppl Table 2), indicating robust de novo thymopoiesis. Although CMV, EBV, and adenovirus viremia were not detected at any time, the patient exhibited BK viremia, consistent with BK virus-specific T cell activity, which was demonstrable by IFNγ Enzyme-linked immunospot (ELISpot) assay

(Millipore Sigma™) at ~6-months post-BMT (Fig 3D). Mitogen testing (PWM and PHA stimulation) revealed normal responses (data not shown). The patient established normal IgA, IgG, and IgM levels, allowing discontinuation of IVIG supplementation ~16 months, followed by initiation of full vaccination ~2 years post-BMT. By three years post-BMT, vaccine responses were detected against tetanus and several of the 16 tested pneumococcal serotypes, and in 2022, against SARS-CoV-2 vaccination (data not shown). Since BMT, radiographical pneumonia has not recurred, and no autoimmune events were noted.

Hypo-responsiveness to host following systemic IST withdrawal

At 2 years post-BMT (off IST for ~8 months), circulating T cells (~99% donor) displayed reduced proliferation against host dendritic cells (hDCs) in the mixed lymphocyte reaction (MLR) assay (Fig 3A) compared to graft T-cells (gT), isolated pre-BMT, which maintained robust proliferation against hDCs (p=0.002) (Fig. 4A). Simultaneously, circulating T-cells responded vigorously to third-party antigen presenting cells (APCs) (Fig. 4A). Similarly, hDCs effectively stimulated third-party T-cells (Fig 4A). By examining the relative ratio of anti-host proliferative capacity to anti-3rd party APC, the tolerant T cells at 2-years post-BMT exhibited a much lower ratio (0.15) compared to graft T-cells (ratio =1.9) (Fig 4A), demonstrating more than 10-fold diminished anti-host proliferative responses towards host DCs by the time of clinical tolerance (Tol). Cytokines detected from these MLR supernatants also reflected hyporeactivity towards the recipient (Fig 4B), mirroring T-cell proliferation results (Fig 4A), and were comparable to anti-self MLR dataset from healthy volunteers (Fig 4E). In contrast, the same T cells displayed vigorous cytokine secretion against 3rd party APCs, including IL-2, IL-13, and most notably IFNγ (Fig 4B). Graft T cells, in comparison, showed robust secretion of these cytokines in response to hDCs (Fig 4C).

Attempts to restore anti-host alloreactivity by *in vitro* modulations at tolerant timepoint

To explore potential peripheral mechanisms associated with clinical tolerance, we depleted Tregs *in vitro* from the patient's T cells prior to MLR assay (21). Rebound T-cell proliferation was not detectable in samples drawn 2-years post-BMT (Fig 4A, 4B), indicating the lack of Treg role sustaining tolerance at this stage. Similarly, the addition of anti-IL-10R blocking antibody to

MLR assay, intended to interfere with Treg and Tr1 cell functions (22), failed to enhance anti-host responses (Fig 4A,4B).

Low dose exogenous IL-2 added to the MLR (23) to test for anergy led to modest increase in anti-host T-cell proliferation compared with cultures without it (p=0.07) (Fig 4A). Nevertheless, similar increase in proliferation was observed utilizing the same *in vitro* modulation of autologous MLR from healthy volunteers (Fig 4D), (p=0.06).

Neither Treg depletion nor IL-10R blockade resulted in increased IL-2 or IFNγ levels (Fig 4B). A slight increase in IL-13 (79pg/mL) was observed at the tolerant stage (Fig 4B). Meanwhile, low dose IL-2 supplementation increased the secretion of IL-13 (177pg/mL), but this level remained far below that observed in response to 3rd party APC (3160pg/mL) (Fig 4B).

Tracking host-reactive clones by TCRβ repertoire sequencing

T-cell clones with anti-host reactivity (N°=99) (Fig 5B) from the original unprocessed VB marrow graft (1E+05 purified T cells) were identified following their *in vitro* expansion in MLR assay in response to host DCs (Fig 5A). These clones became undetectable from the circulation by 6-months post-BMT (Fig 5B). All but one (at only 0.03% frequency) of these T-cell clones remained undetectable after Tacrolimus was fully withdrawn (Fig 5B). At 6 months post-BMT, while the patient was still receiving Tacrolimus, 'new' host-reactive T-cell clones emerged in the circulation (N°=171) (Fig 5D). Notably, these clones were not amongst the original host-reactive clones present in the VB graft (Fig 5C). Most of these clones also disappeared over time, while the remaining ones became greatly diminished in read frequency and remained at very low frequency even after withdrawal of Tacrolimus (Fig 5D). Supplementing the MLR microcultures with low dose of IL-2 neither prevented the disappearance of alloreactive T-cell clones (Fig 5B, Fig 5D) nor impacted the diminution of the read frequency (mean=0.01% at 2 years) of the remaining 'new' host-reactive T-cell clones (N°=54 in 2yrsT+hDC, N°=47 in 2yrsT+hDC+IL2, or N°=73 in 2yrs PBMC), arguing against significant role for anergy (Fig 5B, 5D).

Analysis of signaling pathways in T cells and monocytes at status of clinical tolerance

We compared the gene expression profiles and signaling pathways of the patient's circulating T cells (~99% donor) at the tolerant stage 2-years post-BMT (Tol T) with T cells from the original unmodified marrow graft (gT). The comparison was conducted following *in vitro* stimulation

with hDCs or through direct analysis of cells isolated from the circulation or from the marrow graft. Using Gene Set Enrichment Analysis (GSEA) to compare tolerant circulating T cells at 2 years with gT cells stimulated with hDCs, we identified 22 significantly differentially expressed pathways. Amongst these, 15 were downregulated, exemplified by 'Allograft Rejection' pathway (Fig 6A), 'IL2/STAT5 signaling', 'IFNγ response', 'G2M checkpoint', 'IFNα response', and 'mTORC1 signaling' pathways (Fig 6B).

By using IPA software, we identified 44 pathways with significant differences, contrasting the patient's tolerant T-cells to graft T cells after each were stimulated with hDCs. Inhibited pathways (negative z-score) were exemplified by 'Th1 pathway', 'Cyclins and cell cycle regulation', and 'Granzyme B Signaling'. Conversely, tolerant T cells exhibited activation (positive z-score) of pathways, such as 'cAMP response element-binding protein (CREB) in neurons', 'Ferroptosis Signaling', and 'Phagosome Formation' (Fig 7A, Suppl Table 7). IPA also revealed distinct patterns of signaling pathways in the patient's circulating tolerant T cells alone compared with graft T cells alone, despite both being of donor origin (Fig 7B, Suppl Table 8). There was dichotomy in CREB signaling when tolerant T cells and graft T cells were compared with each other dependent on exposure to hDC or not. Notably, CREB signaling was relatively quiescent (z-score: -8) when Tol T were compared to gT cells without any hDC stimulation while it became more active (z-score: 3) in tolerant T cells compared to graft T after exposure to hDCs by each (Suppl Tables 7 and 8).

At 2-years post-BMT, the patient's circulating CD14+ monocytes (~10-11% donor by FC) were sorted for isolating donor from host monocytes (purity: ~93% or ~100%, respectively) (Suppl Fig 1) and were subjected to RNA-sequencing (RNA-seq) analysis. Distinct patterns of the pathway activities were seen, when comparing co-existing donor and host monocytes (Fig 8A left column, Suppl Table 9), and these patterns differed from those observed pre-BMT (Fig 8A right column). We highlighted 77 out of 251 (Suppl Table 9) pathways that showed statistically significant differences between donor and host monocyte (dMono; hMono) (Fig 8A). Circulating hMono showed relatively higher activation for several pathways, exemplified by 'p53 signaling', 'TGFβ signaling' 'Ferroptosis signaling', 'Immunogenic cell death signaling', 'Macroautophagy', 'FcγR-mediated phagocytosis in Macrophages and Monocytes', 'Necroptosis signaling', 'Macrophage classical activation signaling', 'IL-10 signaling', and 'Microautophagy signaling' pathways (Fig 8B, listed in Suppl Table 9). Conversely, dMono displayed higher

activation for the pathways such as 'CREB signaling in Neurons', 'Granzyme A signaling', and 'Lymphotoxin β receptor' (Fig 8C, listed in Suppl Table 9).

Discussion

We present what we believe to be the first successful human case of durable engraftment and immune competence in a recipient of deceased-donor vertebral bone marrow. Notably, the patient had received BOLT from the same donor a few months earlier. Persistent mixed myeloid chimerism, despite only 1 of 8 HLA-match at allele level, paired with 97-99% T-cell chimerism, has enabled rejection free, stable pulmonary function, protective immunity, and absence of GvHD for over 8 years without IST. The VB marrow graft was recovered hours after cross-clamping and underwent extensive processing prior to cryopreservation. Durable engraftment from the VB graft was feasible despite reduced-intensity conditioning with total body irradiation (TBI) dose ~ 6-fold lower than myeloablative antileukemic regimens, suggesting that reduced-intensity dosing will also be suitable for patients with more host T cells, while the dose reduction can still protect recipients from potential co-morbidities. Protective immunity-without autoimmunity- towards past and new microbes has been sustained for over 8 years, including protective responses to vaccinations.

There have been three prior reports of iliac crest bone marrow transplant from deceased donors. All were performed following standard aspiration technique from the iliac crest of brain-dead donors with either intact circulation or within minutes of the cessation of heart beats. Durable hematopoiesis, immune competence, and tolerance were not evaluable in the report by Blazar et al (24) with the recipient death occurring on day +86 due to GvHD complications. In the case reported by Kapelushnik et al (25), the donor was a related HLA-matched sibling, and the patient was followed only until 8 months post-BMT, although medication-free survival was noted. The third case was our previously published report (21), which described 4-years follow-up demonstrating sustained engraftment, immune competence, and tolerance after receiving T-cell-depleted, cryopreserved BMT from a 4 of 8 -HLA-matched unrelated donor. Years after undergoing BOLT and BMT, that patient was recognized to have Artemis-deficiency as a radiation sensitive type of SCID due to DCLRE1C gene mutation (26), which could explain 100% donor chimerism at all times, following a single fraction of 200cGy TBI and a single dose

of thiotepa (21). She is now >15 years after BMT with no change in the tolerance status, per direct communication.

The infused VB marrow graft in this report was depleted of CD3+ T and CD19+ B cells, thereby preserving hematopoietic and immune progenitors that were recognized decades ago to be biologically suitable for HSCT (27-30). A small dose of DLI, encompassing the entire donor T cell repertoire, was infused ~2 months post-BMT to alleviate CD3 lymphopenia and boost donor T cell chimerism. By 6 months post-BMT, new donor-derived T cells had also emigrated from the host thymus, identifiable by their broad TCR repertoire diversity, newly measurable sjTREC, and flow cytometric conformation of 'recent thymic emigrants'. Reflecting the low intensity of our regimen and normal host NK cell function, recipient hematopoiesis also recovered. Nevertheless, NK cells, and monocytes of donor origin have persisted at steady levels, fluctuating within the range of 7-12%, while donor B lymphocytes have consistently remained above 60%. There was a temporary alloreactive reaction shortly after DLI, accompanied by donor T cell expansion in the periphery. This was associated with short-lived acute skin GvHD without any systemic inflammation. During this period, the patient was maintained on therapeutic levels (6-10ng/ml) of Tacrolimus. A brief course of prednisone led to rapid clearance of GvHD, while still permitting the rise in donor-derived T-cell numbers and relative chimerism.

Mechanisms of tolerance were interrogated by testing circulating T-cells 2 years after BMT, when clinical tolerance had already been in effect for ~8 months. Host-reactive T-cell clones present in the donor marrow - tracked via TCR-complementarity determining region 3 (CDR3) usage- had all but disappeared by 6 months, except for one miniscule clone detectable at 0.03%, despite the infusion of unselected donor leukocyte ~3.5 months earlier. Even after IL-2 supplementation – to account for potential anergy- these clones remained undetectable. Disappearance of host-specific alloreactive clones led to diminished proliferation and greatly reduced Th1/Th2/IL-17 cytokine secretion against host DCs. Neither Treg depletion nor IL-10 signaling blockade succeeded in restoring anti-host reactivity. Taken together, these findings support clonal T-cell deletion as the major mechanism of establishing host-specific tolerance. Deletion has previously been proposed to play a significant role in sustaining long-term immune tolerance post-BMT (11, 21). Interestingly, while the patient was still on full-dose Tacrolimus in this vastly HLA-mismatched setting, new host-reactive T-cell clones that were not present in the

original marrow graft, were identified at the 6-month post-BMT timepoint, coinciding with the onset of thymopoiesis contributing to the peripheral T-cell pool. Most, but not all, of these 'new' T cell clones also disappeared by 2 years post-BMT, while the remaining ones became detectable at much lower frequencies and were unresponsive to exogenous IL-2, regarding their relative frequency.

Circulating T-cells in the state of clinical tolerance exhibited quiescent gene expression profiles for 'allograft rejection' gene set in bulk RNA-seq analyses in response to host DCs, and inflammatory cytokines were quiescent compared with graft T cells, that displayed robust alloreactivity. Nevertheless, certain active signaling pathways were identifiable in tolerant T cells compared with those in the original graft, suggesting that some of the de novo-generated thymocytes in the periphery may exhibit active, presumably host-restrictive suppression functions. When we queried the overwhelmingly (~90%) host-derived monocytes by RNA-seq analysis, contrasting flow-sorted hMono and dMono at the tolerant state 2 years post-BMT, we found that hMono exhibited relatively higher activation of pathways associated with cell death and/or suppression of immune responses. Taken together, these findings raise the distinct possibility that circulating host monocytes may play an instructive, or at least cooperative, role in suppressing residual host-reactive T-cell clones that have bypassed thymic deletion. Upregulated gene sets in host monocytes may contribute to the sustained activation of putative tolerogenic and/or suppressive donor T cell subsets.

The few RNA-seq and scRNA-seq studies – primarily performed in murine models- have focused on alloreactivity related to rejection and GvHD after transplantation, rather than on long-term tolerance. Bezie et al. (35) reported that *in vitro* expanded FOXP3+Tregs secrete IL-34, which influences the expressions of CSF-1R, SDC1, PTPζ on monocyte subsets; IL-34-treated human PBMCs were shown to reduce aGvHD in immunodeficient NSG mice. This represents an extremely artificial system, unlike our studies, which examined purified T cells without exogenous cytokine bias. Nevertheless, RNA-seq profiles from the patient described here did not show significantly increased IL-34 expression in circulating tolerant, unmanipulated, donor-derived T cells compared with graft T cells that were also free of cytokine modulation (data not shown). Similarly, there was no upregulation of CSF-1R, SDC1, PTPζ in either host- or donor-derived monocytes at 2 years post-BMT, compared with the patient's pre-BMT levels (data not shown).

A few xenogeneic GvHD studies have performed transcriptomic analysis, but none have reported groups of mice that were free of both GvHD and immunosuppression therapy (36). One exception is the Stanford group led by Drs. Bacchetta and Roncarolo, who reported GvHD-free survival in mice; however, these mice received genetically modified 'super Treg' inoculums consisting of human conventional CD4+T cells transduced with lentivirus particles coding for FOXP3, resulting in FOXP3 overexpression far beyond physiological levels. These cells were infused as adoptive cell therapy, adding another layer of engineered and exogenously biased experimental model. In their unique, genetically manipulated system, transcriptomic profiling was performed; however, the authors emphasized that these FOXP3-overexpressing GvHD-suppressive cells exhibit a transcriptomic signature distinct from that of their wild-type counterparts (37).

Despite the marked difference in HLA-matching between the French cohort (38)— in which patients had 8/8 -matched donors—and our case, which included only 1/ 8 matched donor, several immune gene expression findings remain comparable. For example, ICOS overexpression observed in our tolerant T-cell analysis (data not shown) aligns with their findings in the 'primary tolerant' cohort, defined as patients who had never experienced GvHD. However, in contrast to their report of CD23R upregulation, we observed CD23R downregulation in tolerant T cells. Moreover, neither proliferation nor cytokine production in response to host DC was impacted in our tolerance assays (Fig 4) after removal of FOXP3+ regulatory T cells, which appeared to be expanded in French 'primary tolerant' cohort. Nevertheless, we also observed that tolerant T cells had increased expression of ICOS, LEF1, and WNT7A compared with graft T cells—but not CD25—which is similar to their findings in the 'tolerant' cohort. However, we did not detect overexpression of TCF7, or IL10 or CD73 in our resting tolerant T cells versus resting graft T cells. Differences in these genes emerged only after both cell types were exposed to host DC, under which conditions tolerant T cells exhibited relatively increased expression of all 3 genes—similar to the French 'primary tolerant' cohort. In their study, resting PBMCs from tolerant patients were subjected to paired gene-expression analyses compared with their respective donor PBMCs, which differs from our experimental conditions.

In conclusion, durable engraftment and immune competence were demonstrable for the first time in a patient receiving BMT from deceased donor vertebral bone marrow. These findings also have relevance to hematological indications, with opportunities for intensifying the conditioning regimen when the underlying condition justifies it. VB transplant with mixed chimerism was sufficient to establish an immune repertoire that permitted tolerance between recipient and lung allograft. Future studies on subsequent tolerant subjects in an ongoing trial with higher-resolution of single-cell RNA-seq studies could shed further light on potentially novel active tolerogenic T-cell and possibly monocyte subsets as well. Our ongoing prospective clinical trial (NCT01852370) pursues VB transplantation in other forms of PID with parallel mechanistic studies (manuscript in preparation).

Methods

Sex as a biological variable

Since this is a single case report, sex was not considered a primary biological variable. The findings are expected to be relevant to both sexes.

Study design

The primary objective of this single case protocol was to ensure durable hematopoietic engraftment from deceased lung donor bone marrow to establish immune competence. Clinical tolerance was defined as the absence of GvHD or lung rejection, paired with stable donor chimerism without systemic IST for ≥3 months. Initiation of IST withdrawal was permissible once the patient reached >12 months post-BOLT, with no lung rejection, and no grade 2 acute or extensive chronic GvHD for > 3months.

Heparinized peripheral blood samples were collected at baseline (pre-BOLT), post-BOLT/pre-BMT, and at 3-, 6-, 9-, 12-,18-months and beyond for immune reconstitution and immune tolerance studies described below.

Engraftment was clinically quantified using STR assay. Research flow cytometry (FC) assays used donor- and host-specific anti-HLA antibodies. Immune reconstitution was monitored by FC (31), signal joint sjTREC, and TCRβ CDR3 spectratypes (32) to assess donor-derived thymopoiesis.

In vitro tolerance in the GvH direction was tested using purified T lymphocytes to measure proliferation in MLR against host DCs, with parallel cytokine secretion profiling of MLR culture supernatants.(33). TCR clonal frequencies were tracked by monitoring individual alloreactive T-cell clones in unmodified VB marrow graft and in longitudinal patient samples, based on their TCRβ V-D-J sequences. A cut-off read frequency of ≥0.1% above unstimulated T cell frequencies was set for 'Clonal Tracker™' tool of ImmunoSEQ™ Analyzer software_v2 (Adaptive Biotechnologies™, Seattle, WA).

Mechanistic laboratory studies for tolerance required demonstration of hyporeactivity in MLR assays towards host DCs with preserved competence against third-party APCs. Removal of regulatory T cells (Treg) evaluated their role in maintaining tolerance, utilizing IL-2-immunotoxin conjugate (IL-2 IT/ denileukin diftitox) exposure prior to MLR.(33) The contribution of Type-1 regulatory T (Tr1) cell was assessed using an anti-IL-10R blocking antibody (Ab). Low dose exogenous IL-2 (5 IU/mL) was used to test for possible anergy (23).

If there was active suppression by Treg or Tr1 cells, their depletion or IL-10R blockade would revive anti-host T-cell clones to proliferate and secrete IFNγ and other cytokines. In the event of anergy, exogenous IL-2 would similarly reinvigorate host-reactive T-cell clones and potentially unveil 'new', previously unrecognized clones not presented in the VB marrow. Sustained hyporeactivity that was unaffected by any of these manipulations, without upregulated gene expression, would support clonal deletion as the sole mechanism for anti-host tolerance (Suppl Table 4).

Human subject's clinical course pre-BMT

The patient was a fourteen-year-old female at the time of BOLT (September 2015), with IL-7 receptor deficient SCID, characterized by two heterozygote mutations (c589-598 del and c993 del) in the IL-7R alpha chain. The diagnosis was established at 9 years of age following recurrent otitis media and pneumonias associated with lymphopenia after age five years. T-cell lymphopenia (<50-60 cells/μL), along with slightly low number of NK cells (~110/μL) and B cells (~ 110/μL), were noted upon referral to UPMC Children's Hospital in 2013. Serum IgA (~300mg/dl) and IgM (~1000mg/dl) were above the normal range while the patient was on IVIG supplementation for inadequate responses to vaccinations. Cultures of sputa and/or bronchial lavages were positive for alcaligenes, acinetobacter, serratia, pseudomonas, and *Aspergillus*

fumigatus. Progressive hypoxia led to nasal cannula oxygen supplementation and malnutrition necessitated enteral tube feeding. At the time of listing for a lung transplant, the lung allocation score (LAS) was 38. Both the UNOS lung/marrow donor and the patient were blood type O+ and were matched serologically at 2 out of 6 HLA antigens (at HLA-A 02 and HLA-DRB 11), fulfilling the minimum acceptable match by her protocol, testing HLA-A, B, DRB1 loci. However, they were only 1 out of 8 HLA-match at allele level typing (sharing HLA-A 02:01). The donor was cytomegalovirus (CMV) seronegative, while the recipient tested seropositive (presumably reflecting IVIG supplementation), as blood CMV PCR test was negative multiple times. Lung transplant was performed with standard institutional induction and maintenance therapy (Basiliximab, Tacrolimus, MMF and short course glucocorticoids).

Vertebral bone marrow transplant

The marrow suspension prepared from the T11 to L4 vertebral bones (34) was depleted of CD3+ and CD19+ cells on a CliniMACS®Plus instrument (Miltenyi Biotec, Bergisch Gladbach, Germany) (Fig 1) and then cryopreserved along with cells from the iliac crest, which contained approximately 20-fold fewer CD34+ progenitor cells and total nucleated cells (TNC). At 4-month post-BOLT (January 2016), the patient underwent reduced-intensity conditioning (RIC), identical to our previously published case (21), consisting of 200cGy TBI x1, 200mg/msq thiotepa x1, alemtuzumab (0.5mg/kg), and horse ATG. The CD3/CD19-depleted bone marrow (CliniMACS®), containing 5E+06 CD34+progenitor cells/kg and 8E+04 CD3+ T cells/kg was thawed and infused on transplant day. Tacrolimus and low-dose Prednisone were continued for lung rejection and GvHD prophylaxis. Irradiated granulocytes from healthy volunteer donors were infused four occasions during the expected neutropenic period, until day+11 post-BMT. The patient received intravenous piperacillin/tazobactam together with inhaled tobramycin daily for two weeks. Inpatient fungal prophylaxis consisted of a combination of voriconazole and caspofungin. Voriconazole was continued in the outpatient setting. Low-dose heparin at 100U/kg/day and ursodiol were used for veno-occlusive disease prophylaxis. Due to persistent T-cell lymphopenia (mostly host origin), the patient received UNOS donor leukocyte infusion (DLI) approximately ten weeks after BMT (containing 5E+04 CD3+ T cells/kg). Tacrolimus taper started ~12 months post-BMT and was fully discontinued by 16-month.

Assessment of engraftment

Research grade flow cytometry (FC) was performed on surface stained PBMCs following the manufacturer's instructions, using CD45-PerCP (Cat#347464, Becton Dickinson™ [BD], NJ), CD3-BV421 (Cat#562426, BD™), CD19-BV510 (Cat#562947, BD™), and CD56-PE-Cy7 (Cat#318318,BioLegend® San Diego, CA), along with donor-specific HLA-B12-FITC Ab (Cat#FH0066) and host-specific HLA-A9-Biotin conjugated Ab (Cat#BIH0964) (both from One Lambda™ Solutions at Thermo Fisher Scientific, Waltham, MA). Streptavidin-APC (Cat#016-130-084) (Jackson ImmunoResearch Laboratories™ Inc. Wests Grove, PA) was used as secondary Ab. Clinically reported DNA based chimerism testing was performed by the Histocompatibility Lab at UPMC Lab Services employing STR PCR assays on PB and immunomagnetically purified CD3+ and CD33+ cells.

Determination of lymphocyte reconstitutions using flow cytometry

Absolute T-, B-, and NK-cell numbers were tested using flow cytometry (FC) TruCount™ assay (BD Bioscience™) following the manufacturer's instructions. The Abs included Multitest™ (CD45-PerCP, CD3-FITC, CD4-APC, CD8-PE) (Cat#340499, BD™), CD19-BV421 (Cat#302234, BioLegend™), CD56-PE-Cy7 (Cat#318318, BioLegend™), CD16-BV510 (Cat#563830, BD™), and CD14-APC-H7 (Cat#398708, BioLegend™). CD4+ naïve T cells were examined using FC Abs including CD3-FITC (Cat#555332, BD™), CD4-BV510 (Cat#562970, BD™), CD8-APC-H7 (Cat#560179, BD™), CD45RA-PE-Cy7 (Cat#560675, BD™), and CD62L-APC (Cat#559772, BD™), and were defined as positive for CD3/CD4/CD45RA/CD62L.

Mixed lymphocyte reactions and Bio-plex™ cytokine assay

Modified MLR assays were performed at scheduled intervals: pre-BMT for graft testing, and at 3, 6, 9, 12, and 18 month, as well as 2 years post-BMT, employing purified T cells from the patient (PtT) or the VB marrow graft (gT) and host dendritic cells (hDC) besides IM9, a 3rd party commercial professional APC line.(21, 33) Cryopreserved supernatants collected prior to ^{3}H-Thymidine pulse were cryopreserved and batched before testing for Th1/Th2/IL-17

cytokines, using Bio-Plex™ kits (Bio-Rad™, Hercules, CA) following the manufacturer's instructions.

Examination of sjTREC and TCRβ CDR3 size spectratyping

The sjTREC and TCRβ CDR3 size spectratyping were performed as we described previously (32). The overall complexity of TCRβ subfamilies was quantitated by the spectratype complexity score (SCS), as published (32).

Quantification of IFNγ secreting T-cell response using Enzyme-linked immunospot (ELISpot) assay

ELISpot assay was performed according to the manufacturer's brochure (Millipore-Sigma™).

TCRβ repertoire immunosequencing and RNA-sequencing

TCRβ repertoire 'immunosequencing' and bulk RNA-sequencing were performed by Adaptive Biotechnologies™ (Seattle, WA), or at the Health Sciences Sequencing Core at UPMC Children's Hospital of Pittsburgh, respectively.

Statistical analysis

Paired *t*-tests with Bonferroni multiple-comparison adjustment were used for MLR assays (Figs 4A, 4D). Student's *t*-tests were applied to the cytokine data analysis (Fig 4F). The Mann-Whitney nonparametric test was used to compare clonal T-cell frequencies (Fig 5B, 5D). Statistical analyses were performed using GraphPad Prism™ software_v10 (GraphPad™ Software Inc, San Diego, CA). All tests were 2-tailed, and the results were considered statistically significant when the *p*-value was less than 0.05.

Study approval: This study was approved by the Institutional Review Board (IRB) of University of Pittsburgh (FDA-IND 15414, Clinical treatment: Pitt IRB Pro113040207; Mechanistic studies: Pitt IRB PRO16010311; PRO19070076; PRO1108066), and written informed consent was obtained from all participants prior to their involvement.

Data availability: Clinical data is available from the corresponding author. RNA-seq raw data was deposited into GEO database (Accession number: GSE305710), while MLR, Bioplex-cytokine assays, and TCRβ-seq data are provided in .XLS format. TCRβ-seq FASTA data will be made available upon request from corresponding author.

Author contributions

P.Sz. designed the study, obtained IRB and FDA approval, treated the patient, supervised VBM processing, designed laboratory experiments, reviewed medical and laboratory data and wrote the manuscript. **X.C.** contributed to lab experimental design, supervised immune monitoring experiments, performed MLR, FACS, sjTREC, TCR spectratyping, Bio-plex, DNA-RNA preparations for ImmunoSEQ and RNA-seq, conducted data analysis and wrote first draft of the manuscript and laboratory analyses. **M.G.M.** oversaw infectious disease monitoring and provided clinical antimicrobial advice, **M.H**. performed FACS, ELISpot, sjTREC, TCR spectratyping, and MLR assays, and conducted data analysis. **E.G.** contributed to sample collection, performed FACS, sjTREC, TCR spectratyping assays. **Z.A.** contributed to sample collection and performed FACS analysis. **H.M.S.** oversaw vertebral marrow processing, CD3/CD19 depletion, QC steps and it's cryopreservation. **S.M.** oversaw and managed all clinical and laboratory research regulatory procedures, coordinated research distribution of samples. **A.P.** referred the patient and provided prior clinical supportive care. **D.R.** oversaw processing and contributed to the interpretation of RNA-seq data. **A.C**. contributed to interpretation of IPA data and partially joined the analysis. **P.D.W**. performed lung transplant surgical procedures, **J.E.S.** and **G.K**. coordinated pulmonary and overall medical care before and after lung transplant. All the authors reviewed, edited, and provided final approval for the manuscript.

Funding support: This study was supported by UPMC Children's Hospital 'Start Up' fund to PSz. for supporting laboratory research activities.

Acknowledgments

We are indebted to the patient and their mother, as well as the physicians and nurses at UPMC Children's Hospital for their exceptional clinical care. We also extend our appreciation to the Stem Cell Laboratory for the processing and cryopreservation of the vertebral marrow graft. We

are grateful to Drs. Craig Byersdorfer and Randy Windreich along with Jason Rowan for assisting in vertebral log recovery. We gratefully acknowledge the UPMC Clinical Laboratories Histocompatibility Lab for HLA-typing and serial chimerism testing, the staff and scientists at Adaptive Biotechnologies™ Inc. for performing TCRβ Immunosequencing and providing consultation on the application of ImmunoSEQ™ Analyzer software. We are grateful to the staff and scientists at the Genomics Research Core at the University of Pittsburgh for conducting the TCR CDR3 spectratyping assay. Additionally, we thank the staff at UPMC Children's Hospital RNA-seq core for their precision technologies including Ms. Chaparala, S. at Molecular Biology Information Service at Health Sciences Library System of University of Pittsburgh. We thank the 'Center for Research Computing and Data' at the University of Pittsburgh for providing services towards RNA-seq analysis. We thank UPMC Children's Hospital 'Start Up' fund to PSz. for supporting laboratory research works.

References

1. Stiehm ER, Chin TW, Haas A, and Peerless AG. Infectious complications of the primary immunodeficiencies. *Clin Immunol Immunopathol.* 1986;40(1):69-86.
2. Notarangelo LD, Plebani A, Mazzolari E, Soresina A, and Bondioni MP. Genetic causes of bronchiectasis: primary immune deficiencies and the lung. *Respiration.* 2007;74(3):264-75.
3. Bustamante J, Zhang SY, von Bernuth H, Abel L, and Casanova JL. From infectious diseases to primary immunodeficiencies. *Immunol Allergy Clin North Am.* 2008;28(2):235-58, vii.
4. Kulkarni HS, Cherikh WS, Chambers DC, Garcia VC, Hachem RR, Kreisel D, et al. Bronchiolitis obliterans syndrome-free survival after lung transplantation: An International Society for Heart and Lung Transplantation Thoracic Transplant Registry analysis. *J Heart Lung Transplant.* 2019;38(1):5-16.
5. Napoli C, Benincasa G, Fiorelli A, Strozziero MG, Costa D, Russo F, et al. Lung transplantation: Current insights and outcomes. *Transpl Immunol.* 2024;85:102073.
6. Thompson ML, Flynn JD, and Clifford TM. Pharmacotherapy of lung transplantation: an overview. *J Pharm Pract.* 2013;26(1):5-13.
7. Thangavelu G, and Blazar BR. Achievement of Tolerance Induction to Prevent Acute Graft-vs.-Host Disease. *Front Immunol.* 2019;10:309.
8. Adams DH, Sanchez-Fueyo A, and Samuel D. From immunosuppression to tolerance. *J Hepatol.* 2015;62(1 Suppl):S170-85.
9. Pham SM, Keenan RJ, Rao AS, Fontes PA, Kormos RL, Abu-Elmagd K, et al. Perioperative donor bone marrow infusion augments chimerism in heart and lung transplant recipients. *Ann Thorac Surg.* 1995;60(4):1015-20.

10. Andreola G, Chittenden M, Shaffer J, Cosimi AB, Kawai T, Cotter P, et al. Mechanisms of donor-specific tolerance in recipients of haploidentical combined bone marrow/kidney transplantation. *Am J Transplant.* 2011;11(6):1236-47.
11. Morris H, DeWolf S, Robins H, Sprangers B, LoCascio SA, Shonts BA, et al. Tracking donor-reactive T cells: Evidence for clonal deletion in tolerant kidney transplant patients. *Sci Transl Med.* 2015;7(272):272ra10.
12. Leventhal J, Abecassis M, Miller J, Gallon L, Ravindra K, Tollerud DJ, et al. Chimerism and tolerance without GVHD or engraftment syndrome in HLA-mismatched combined kidney and hematopoietic stem cell transplantation. *Sci Transl Med.* 2012;4(124):124ra28.
13. Scandling JD, Busque S, Dejbakhsh-Jones S, Benike C, Sarwal M, Millan MT, et al. Tolerance and withdrawal of immunosuppressive drugs in patients given kidney and hematopoietic cell transplants. *Am J Transplant.* 2012;12(5):1133-45.
14. Leventhal JRE, M. J. Yolcu, E. S. Bozulic, L. D. Tollerud, D. J. Mathew, J. M. Konieczna, I. Ison, M. G. Galvin, J. Mehta, J. Badder, M. D. Abecassis, M. M. I. Miller, J. Gallon, L. Ildstad, S. T. Immune reconstitution/immunocompetence in recipients of kidney plus hematopoietic stem/facilitating cell transplants. *Transplantation.* 2015;99:288-98.
15. Bertaina A, Grimm PC, and Weinberg K. Sequential Stem Cell-Kidney Transplantation in Schimke Immuno-osseous Dysplasia. Reply. *N Engl J Med.* 2022;387(9):860.
16. Busque S, Scandling JD, Lowsky R, Shizuru J, Jensen K, Waters J, et al. Mixed chimerism and acceptance of kidney transplants after immunosuppressive drug withdrawal. *Sci Transl Med.* 2020;12(528).
17. Podesta MA, and Sykes M. Chimerism-Based Tolerance to Kidney Allografts in Humans: Novel Insights and Future Perspectives. *Front Immunol.* 2021;12:791725.
18. Sykes M. Leveraging the lymphohematopoietic graft-versus-host reaction (LGVHR) to achieve allograft tolerance and restore self tolerance with minimal toxicity. *Immunother Adv.* 2023;3(1):ltad008.
19. Sayegh MH, Fine NA, Smith JL, Rennke HG, Milford EL, and Tilney NL. Immunologic tolerance to renal allografts after bone marrow transplants from the same donors. *Ann Intern Med.* 1991;114(11):954-5.
20. Helg C, Chapuis B, Bolle JF, Morel P, Salomon D, Roux E, et al. Renal transplantation without immunosuppression in a host with tolerance induced by allogeneic bone marrow transplantation. *Transplantation.* 1994;58(12):1420-2.
21. Szabolcs P, Buckley RH, Davis RD, Moffet J, Voynow J, Antony J, et al. Tolerance and immunity after sequential lung and bone marrow transplantation from an unrelated cadaveric donor. *J Allergy Clin Immunol.* 2015;135(2):567-70.
22. Serafini G, Andreani M, Testi M, Battarra M, Bontadini A, Biral E, et al. Type 1 regulatory T cells are associated with persistent split erythroid/lymphoid chimerism after allogeneic hematopoietic stem cell transplantation for thalassemia. *Haematologica.* 2009;94(10):1415-26.
23. Dure M, and Macian F. IL-2 signaling prevents T cell anergy by inhibiting the expression of anergy-inducing genes. *Mol Immunol.* 2009;46(5):999-1006.
24. Blazar BR, Lasky LC, Perentesis JP, Watson KV, Steinberg SE, Filipovich AH, et al. Successful donor cell engraftment in a recipient of bone marrow from a cadaveric donor. *Blood.* 1986;67(6):1655-60.

25. Kapelushnik J, Aker M, Pugatsch T, Samuel S, and Slavin S. Bone marrow transplantation from a cadaveric donor. *Bone Marrow Transplant.* 1998;21(8):857-8.
26. Moshous D, Callebaut I, de Chasseval R, Corneo B, Cavazzana-Calvo M, Le Deist F, et al. Artemis, a novel DNA double-strand break repair/V(D)J recombination protein, is mutated in human severe combined immune deficiency. *Cell.* 2001;105(2):177-86.
27. Mugishima H, Terasaki P, and Sueyoshi A. Bone marrow from cadaver donors for transplantation. *Blood.* 1985;65(2):392-6.
28. Sharp TG, Sachs DH, Matthews JG, Maples J, Woody JN, and Rosenberg SA. Harvest of human bone marrow directly from bone. *J Immunol Methods.* 1984;69(2):187-95.
29. Rybka WB, Fontes PA, Rao AS, Winkelstein A, Ricordi C, Ball ED, et al. Hematopoietic progenitor cell content of vertebral body marrow used for combined solid organ and bone marrow transplantation. *Transplantation.* 1995;59(6):871-4.
30. Soderdahl G, Tammik C, Remberger M, and Ringden O. Cadaveric bone marrow and spleen cells for transplantation. *Bone Marrow Transplant.* 1998;21(1):79-84.
31. Szabolcs P, Park KD, Reese M, Marti L, Broadwater G, and Kurtzberg J. Coexistent naive phenotype and higher cycling rate of cord blood T cells as compared to adult peripheral blood. *Exp Hematol.* 2003;31(8):708-14.
32. Chen X, Barfield R, Benaim E, Leung W, Knowles J, Lawrence D, et al. Prediction of T-cell reconstitution by assessment of T-cell receptor excision circle before allogeneic hematopoietic stem cell transplantation in pediatric patients. *Blood.* 2005;105(2):886-93.
33. Szabolcs P, Park KD, Marti L, Deoliveria D, Lee YA, Colvin MO, et al. Superior depletion of alloreactive T cells from peripheral blood stem cell and umbilical cord blood grafts by the combined use of trimetrexate and interleukin-2 immunotoxin. *Biol Blood Marrow Transplant.* 2004;10(11):772-83.
34. Gorantla VS, Schneeberger S, Moore LR, Donnenberg VS, Zimmerlin L, Lee WP, et al. Development and validation of a procedure to isolate viable bone marrow cells from the vertebrae of cadaveric organ donors for composite organ grafting. *Cytotherapy.* 2012;14(1):104-13.
35. Bezie S, Freuchet A, Serazin C, Salama A, Vimond N, Anegon I, et al. IL-34 actions on FOXP3+ Tregs and CD14+ monocytes control human graft rejection. *Front Immunol*. 2020;11:1496.
36. Gilman KE, Cracchiolo MJ, Matiatos AP, Davini DW, Simpson RJ, Katsanis E, Partially replacing cyclophosphamide with bendamustine in combination with cyclosporing A improves survival and reduces xenogeneic graft-versus-host-disease. *Front Immunol*. 2023;13:1045710
37. Sato Y, Passerini L, Piening BD, Uyeda MJ, Goodwin M, Gregori S, et al. Human-engineered Treg-like cells suppress FOXP3-deficient T cells but preserve adaptive immune responses in vivo. *Clin Transl Immunol*. 2020;9(11):e1214.
38. Dubouchet L, Todorov H, Seurinck R, Vallet N, Van Gassen S, Corneau A, et al. Operationa tolerance after hematopoietic stem cell transplantation is characterized by distinct transcriptional, phenotypic, and metabolic signatures. *Sci Transl Med*. 2022;14(633):eabg3083.

Figure legend:

Figure 1. Clinical scheme and study design: After the eligibility of this study protocol was confirmed and listed with UNOS, a suitable donor was identified (**July. 2013 to Sept. 2015**). Vertebral bodies were surgically recovered before patient received bilateral orthotopic lung transplant (**BOLT) (Sept. 2015).** The vertebral bodies were dissected, crushed, and filtered within 48 hours after receiving them. Following CD3+T/CD19+B cell depletion using CliniMACS®, vertebral bone marrow (**VBM**) was collected and cryopreserved. A few months later (minimum of 8 weeks post-BOLT), conditioning regimen was performed, followed by BM transplantation (**BMT) (Jan. 2016, day 0)**. On day +13 post-BMT (**Feb. 2016**) donor engraftment was confirmed. To overcome T-cell lymphopenia associated with the emergence of host T cells (73% host at 2 months), the patient received donor leukocyte infusion (**DLI, April. 2016, day +69**). The immunosuppressive treatment (**IST**) was maintained until approximately 1-year post-BMT.

Figure 2. Longitudinal monitoring of donor cell chimerism and pulmonary function tests. A) Pulmonary function test results prior to BOLT and over time thereafter. The y-axis depicts % predicted values. Arrows indicate the timing of BOLT (Sept 2015) and BMT (January 2016). **B)** STR chimerism for whole peripheral blood (PB) leukocytes; **C**) Chimerism of CD3+T cells; **D)** Chimerism of myeloid cells, including CD33+ cells tested by STR assay and monocytes tested by flow cytometry (FC); **E)** Chimerism of CD19+B cells, and **F)** Chimerism of CD56+ NK cells. The y-axis depicts % donor contribution at various time points post-BMT, as indicated on the x-axis. △ represents donor chimerism measured byFC on PB leukocytes, □ indicates data tested using FC on bronchoalveolar lavage (BAL), and ○ displays chimerism data tested by STR assay on purified CD3+ and CD33+ cells from PB. ● indicates STR assay on whole PB leukocytes. The antibodies (Abs) used for FC chimerism include CD45-PerCP, CD3-BV421, CD19-BV510, CD56-PE-Cy7 (BioLegend® San Diego, CA), along with donor-specific HLA-B12-FITC Ab and host-specific HLA-A9-Biotin conjugated Ab (both from One Lambda™ Solutions at Thermo Fisher).

Figure 3. Immune reconstitution post-BMT. A) Numerical lymphocyte reconstitution before BMT (including baseline [BSL] and post-BOLT/pre-BMT) and during post-BMT thymopoiesis. The y-axis shows absolute cell numbers (N°)/μL over time (x-axis). **B)** Thymic output assessed

by sjTREC and TCRβ spectratype over time. The left y-axis represents the spectratype complexity score (SCS), while the right y-axis shows sjTREC copies/10^5 T cells. **C)** Acquisition of TCR repertoire diversity. Each box represents a 'family' of T-cell clones with a specific TCR Vβ. Individual peaks correspond to distinct TCRs based on their CDR3 length. The cumulative number of peaks is expressed as SCS, shown below each figure at the respective time-point. **D)** T-cell responses illustrated by IFNγ ELISpot images following stimulation with overlapping peptide pools from BK virus and CMV at 6 months post-BMT. Both donor and recipient were CMV-negative.

Figure 4. Anti-host proliferation by donor T cells in MLR and cytokine profiles contrasting circulating donor-derived T cells at tolerant state with graft T cells. A) Proliferative responses of graft T cells (gT) or circulating patient T cells (2yrs PtdT, all donor-derived) obtained at clinical tolerance(2yrs post-BMT) against host dendritic cells (hDCs), with or without *in vitro* modifications intended to 'break tolerance', including addition of low dose IL2 (▼), Treg depletion using IL2-conjugated immunotoxin (IL2-IT) (◆), and anti-IL10R antibody treatment (⬣). Positive controls included gT or circulating T cells tested against 3rd party antigen-presenting cells (APCs) and 3rd party T cells tested against hDCs. 'Ratio' represents T+hDC/T+3rd party APC. The y-axis shows ^{3}H-thymidine incorporation count per minute (CPM). **B)** Cytokine profiles generated from MLR (shown in **A)** culture supernatants of circulating donor-derived T cells (2yrs PtdT) at clinical tolerance (2yrs post-BMT), alone and stimulated with hDC ±modifiers; **C)** Cytokine profiles generated from MLR (shown in **A)** culture supernatants of graft T cells (gT), alone and stimulated with hDCs ±modifiers; **D)** Autologous MLR assay for healthy volunteers (HVOL, n=6) T cells alone and against self-DC under the same conditions as in **A)**. Significant or near-significant p-values (≤0.05) by paired *t*-test are indicated. NS represents a 'non-significant' result. **E)** Cytokine profiles generated from MLR (shown in D) culture supernatants of HVOL T cells alone and stimulated with self-DCs ±modifiers. The y-axis represents *in vitro* culture conditions; the top x-axis lists tested cytokines. Each square reflects the mean normalized cytokine value (pg/mL, with hDC value subtracted) for each condition. Color scale bar shown on the right. **F)** Comparison of IL2 and IFNγ secretion by gT cells, circulating T cells at 2 years post-BMT (2yrs PtdT), and HVOL T cells, after 5-day stimulation with hDCs (for gT and 2yrs PtdT) or self-DCs (for HVOL T). Paired *t*-tests with Bonferroni multiple-comparison adjustment were used for MLR assays. Student's t-tests were

applied to the cytokine data analysis. All analyses were performed with 2-tail tests, and the results were considered statistically significant when the *p*-value was less than 0.05.

Figure 5. Tracking host-reactive T-cell clones using 'Clonal Tracker™' tool in ImmunoSEQ™ Analyzer Software_v2. A) Identification of host-reactive T-cell clones based on their unique TCRβ CDR3 sequences from pre-BMT bone marrow graft (1E+05 purified T cells) after *in vitro* stimulation with hDCs at 5:1 ratio. Clones with a read frequency ≥ 0.1% (y-axis) compared to unstimulated graft T cells (x-axis) were selected for tracking. **B)** Longitudinal tracking host-reactive T-cell clones (clonal type N°=99) in the patient post-BMT. The y-axis shows % read frequency of each clone type over time (x-axis). Each filled dark red circle represents an individual host-reactive clone type identified amongst graft T cells. Addition of IL-2 to the MLR culture to reverse potential anergy is indicated in red font. **C)** Selection of 'new' alloreactive T-cell clone types (green filled circles) that are ≥ 0.1% frequency and were not identifiable in gT+hDC coculture. **D)** Tracking of these 'new' alloreactive T-cell clones (clonal type N°=171) post-BMT. Numbers at each time point indicate the count of detectable clonal types at any frequency. The Mann-Whitney nonparametric test was used to compare clonal T-cell frequencies. All analyses were performed with 2-tail tests, and the results were considered statistically significant when the *p*-value was less than 0.05.

Figure 6. GSEA signaling pathway analysis comparing circulating T cells (donor origin) in tolerant state with T cells from the donor graft. A) After stimulation with hDCs, the 'allograft-rejection' signaling pathway was downregulated in tolerant T cells (Tol T) 2 years post-BMT (left enrichment plot) compared to graft T-cells containing host-reactive clones pre-BMT (right enrichment plot). Individual genes are displayed on a heatmap, with red indicating upregulation (positive rank matric score) and blue indicating downregulation (negative rank matric score). The color scale bar is shown on the right side of the heatmap. **B)** 12 enrichment plots showing pathways that are either downregulated in tolerant T cells (8 plots, first row) compared to graft T cells (second row) after hDC stimulation. **C)** Four enrichment plots showing pathways upregulated in tolerant T cells compared to graft T cells under the same conditions. The genes were selected based on their false discovery rate (FDR) ≤ 0.05 and $\log_2$ fold changes ≥1 or ≤ -1. Data was analyzed using Gene Set Enrichment Analysis®_v4.3.2 (UC San Diego and Broad Institute, Boston MA). Any signaling pathway was considered significantly altered if its nominal p-value ≤0.05' and/or 'FDR q-value of ≤0.25'. For Figures 6A, relative gene expression

was visualized through 'conditional formatting' in Microsoft Excel™ (Microsoft Corporation, Inc, Seattle, WA).

Figure 7. Signaling pathway analysis contrasting circulating T-cells (donor origin) at tolerant state with T cells from the donor graft. A) Ingenuity Pathway Analysis (IPA) comparing tolerant T cells (Tol T, 99.8% donor origin) collected 2 years post-BMT with bone marrow graft T cells (gT) collected pre-BMT, which possessed potential alloreactivity. Both cell populations were stimulated *in vitro* with hDCs for 7 days. **B)** Heatmap comparison of signaling pathways between tolerant T cells (Tol T, left column) and graft T cells (gT, right column) without *in vitro* stimulation. Each box represents a signaling pathway that is either activated (positive z-score, light yellow for most positive) or inhibited (negative z-score, dark blue for most negative). Pathways are listed on the y-axis, and the color scale bar is shown on the right side of the heatmap.

Figure 8: Comparison of signaling pathways between circulating host and donor monocytes from the same time point using IPA software. **A)** Heatmap comparison of signaling pathways between host monocytes (hMono) and donor monocytes (dMono) collected either from flow cytometrically sorted monocytes using unique and HLA-specific antibodies at 2-years post-BMT (left column) or from patient PB and graft pre-BMT (right column). Each box represents a signaling pathway either activated (positive z-score ≥2, dark red as most positive) or inhibited (negative z-score ≤-2, dark blue as most negative). Pathways are listed on the y-axis, and z-score color scale bar is shown on the right side of the heatmap. **B)** Highlighting 12 pathways from left column of panel **A** that are activated in circulating hMono (left column) relative to circulating dMono (right column). **C)** Highlighting 10 signaling pathways from left column of panel **A** that are quiescent in hMono (left column) compared to dMono (right column).

Supplemental Figure 1. Purity of donor and host monocytes from patient PB collected 2 years post-BMT and purified using FACS sorting. A) Gating strategy for donor and host monocytes before sorting, A1, CD14+monocyte selection; A2. singlet selection; A3. Separation of donor and host monocyte based on donor HLA-specific Ab. **B)** Purity of isolated donor monocytes. B1. CD14+monocytes; B2. Singlet selection; B3. purity of isolated donor monocytes after sorting. **C)** Purity of isolated host monocytes. C1. CD14+monocytes; C2. Singlet selection. C3. purity of host monocytes after sorting.

Supplemental Table 1. Patient chimerism post-BMT (% donor)

Supplemental Table 2. Reconstitution of immune components post-BMT prior to and during thymopoiesis (cell numbers/µL by research FC).

Supplemental Table 3. Potential outcomes and mechanistic interpretation of 'Tolerance' in different MLR setups

Supplemental Table 4. Clinical chronology and graft characteristics

Supplemental Table 5. List of genes and their ranks in the downregulated 'Allograft Rejection' pathway analyzed by GSEA software, contrasting tolerant T cells (Tol T) and graft T cells (gT)[1] after *in vitro* stimulation with hDC.

Supplemental Table 6. Signaling pathway profile analyzed by GSEA software comparing tolerant T cells (2 years post-BMT) and graft T cells after *in vitro* stimulation with hDCs.

Supplemental Table 7. Signaling pathway profiles analyzed by IPA software contrasting circulating donor-derived tolerant T cells (Tol T, 2 years post-BMT) and donor bone marrow graft T cells (gT) after *in vitro* stimulation with hDCs.

Supplemental Table 8. Signaling pathway profiles analyzed by IPA software contrasting tolerant T cells (Tol T, 2 years post-BMT) and bone marrow graft T cells (gT) without any *in vitro* stimulation.

Supplemental Table 9. Signaling pathway profiles analyzed by IPA software contrasting co-existing circulating host and donor monocytes at 2 years post-BMT.

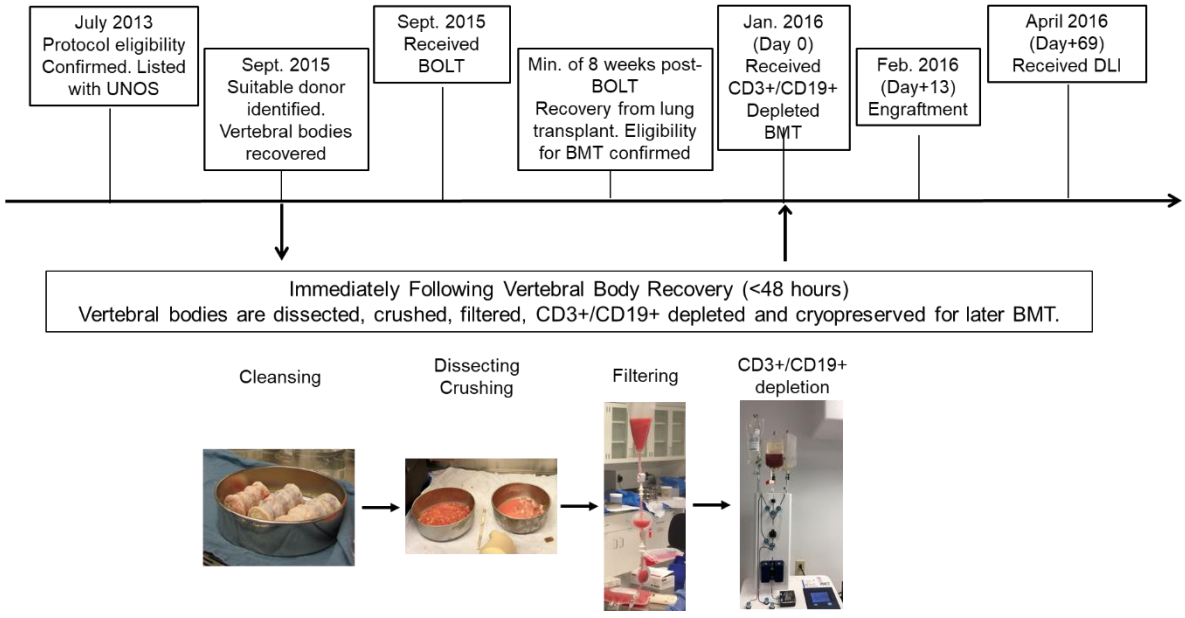

Figure 1. Clinical scheme and study design: After the eligibility of this study protocol was confirmed and listed with UNOS, a suitable donor was identified (**July. 2013 to Sept. 2015**). Vertebral bodies were surgically recovered before patient received bilateral orthotopic lung transplant (**BOLT) (Sept. 2015).** The vertebral bodies were dissected, crushed, and filtered within 48 hours after receiving them. Following CD3+T/CD19+B cell depletion using CliniMACS®, vertebral bone marrow (**VBM**) was collected and cryopreserved. A few months later (minimum of 8 weeks post-BOLT), conditioning regimen was performed, followed by BM transplantation (**BMT) (Jan. 2016, day 0)**. On day

+13 post-BMT (**Feb. 2016**) donor engraftment was confirmed. To overcome T-cell lymphopenia associated with the emergence of host T cells (73% host at 2 months), the patient received donor leukocyte infusion (**DLI, April. 2016, day +69**). The immunosuppressive treatment (**IST**) was maintained until approximately 1-year post-BMT.

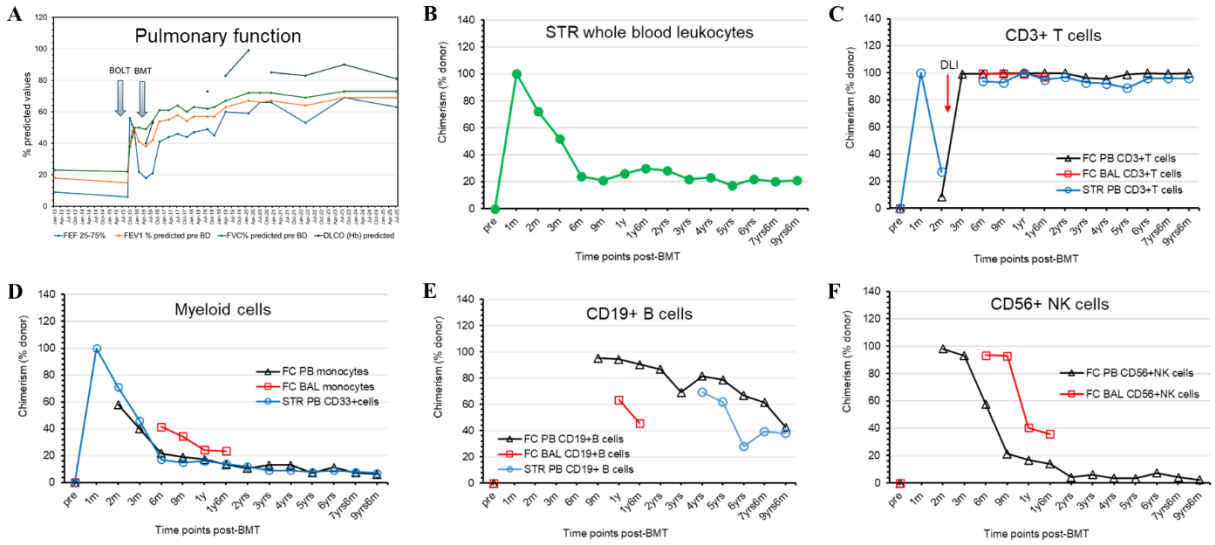

Figure 2. Longitudinal monitoring of donor cell chimerism and pulmonary function tests. A) Pulmonary function test results prior to BOLT and over time thereafter. The y-axis depicts % predicted values. Arrows indicate the timing of BOLT (Sept 2015) and BMT (January 2016). **B)** STR chimerism for whole peripheral blood (PB) leukocytes; **C**) Chimerism of CD3+T cells; **D)** Chimerism of myeloid cells, including CD33+ cells tested by STR assay and monocytes tested by flow cytometry (FC); **E)** Chimerism of CD19+B cells, and **F) Chimerism of** CD56+ NK cells. The y-axis depicts % donor contribution at various time points post-BMT, as indicated on the x-axis. △ represents donor chimerism measured by FC on PB leukocytes, □ indicates data tested using FC on bronchoalveolar lavage (BAL), and ○ displays chimerism data tested by STR assay on purified CD3+ and CD33+ cells from PB. ● indicates STR assay on whole PB leukocytes. The antibodies (Abs) used for FC chimerism include CD45-PerCP, CD3-BV421, CD19-BV510, CD56-PE-Cy7 (BioLegend® San Diego, CA), along with donor-specific HLA-B12-FITC Ab and host-specific HLA-A9-Biotin conjugated Ab (both from One Lambda™ Solutions at Thermo Fisher).

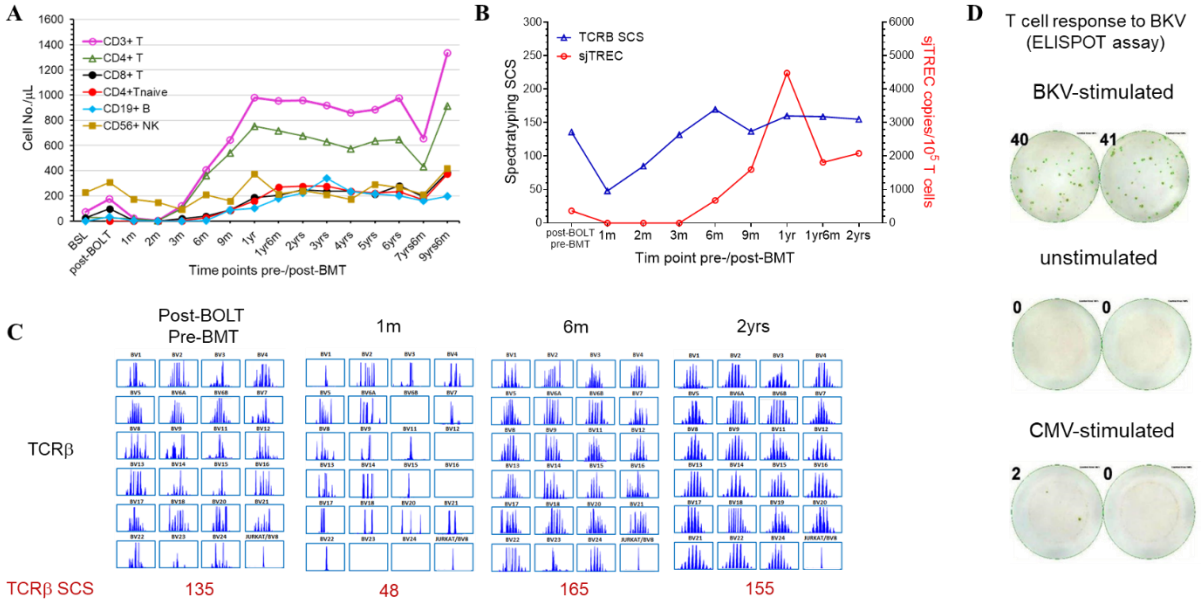

Figure 3. Immune reconstitution post-BMT. A) Numerical lymphocyte reconstitution before BMT (including baseline [BSL] and post-BOLT/pre-BMT) and during post-BMT thymopoiesis. The y-axis shows absolute cell numbers (N°)/µL over time (x-axis). **B)** Thymic output assessed by sjTREC and TCRβ spectratype over time. The left y-axis represents the spectratype complexity score (SCS), while the right y-axis shows sjTREC copies/10^5 T cells. **C)** Acquisition of TCR repertoire diversity. Each box represents a 'family' of T-cell clones with a specific TCR Vβ. Individual peaks correspond to distinct TCRs based on their CDR3 length. The cumulative number of peaks is expressed as SCS,

shown below each figure at the respective time-point. **D)** T-cell responses illustrated by IFNγ ELISpot images following stimulation with overlapping peptide pools from BK virus and CMV at 6 months post-BMT. Both donor and recipient were CMV-negative.

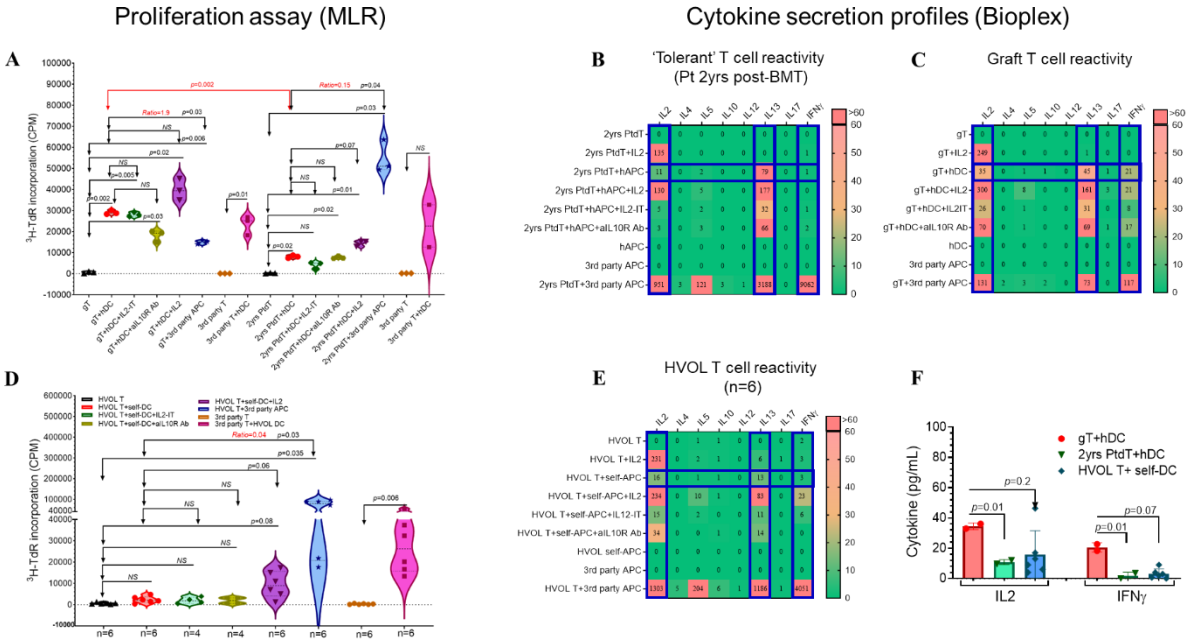

Figure 4. Anti-host proliferation by donor T cells in MLR and cytokine profiles contrasting circulating donor-derived T cells at tolerant state with graft T cells. A) Proliferative responses of graft T cells (gT) or circulating patient T cells (2yrs PtdT, all donor-derived) obtained at clinical tolerance(2yrs post-BMT) against host dendritic cells (hDCs), with or without *in vitro* modifications intended to 'break tolerance', including addition of low dose IL2 (▼), Treg depletion using IL2-conjugated immunotoxin (IL2-IT) (◆), and anti-IL10R antibody treatment (●). Positive controls included gT or circulating T cells tested against 3rd party antigen-presenting cells (APCs) and 3rd party T cells tested against hDCs. 'Ratio' represents T+hDC/T+3rd party APC. The y-axis shows ^{3}H-thymidine incorporation count per minute (CPM). **B)** Cytokine profiles generated from MLR (shown in **A)** culture supernatants of circulating donor-derived T cells (2yrs PtdT) at clinical tolerance (2yrs post-BMT), alone and stimulated with hDC ±modifiers; **C)** Cytokine profiles generated from MLR (shown in **A)** culture supernatants of graft T cells (gT), alone and stimulated with hDCs ±modifiers; **D)** Autologous MLR assay for healthy volunteers (HVOL, n=6) T cells alone and against self-DC under the same conditions as in **A)**. Significant or near-significant p-values (≤0.05) by paired *t*-test are indicated. NS represents a 'non-significant' result. **E)** Cytokine profiles generated from MLR (shown in D) culture supernatants of HVOL T cells alone and stimulated with self-DCs ±modifiers. The y-axis represents *in vitro* culture conditions; the top x-axis lists tested cytokines. Each square reflects the mean normalized cytokine value (pg/mL, with hDC value subtracted) for each condition. Color scale bar shown on the right. **F)** Comparison of IL2 and IFNγ secretion by gT cells, circulating T cells at 2 years post-BMT (2yrs PtdT), and HVOL T cells, after 5-day stimulation with hDCs (for gT and 2yrs PtdT) or self-DCs (for HVOL T). Paired *t*-tests with Bonferroni multiple-comparison adjustment were used for MLR assays. Student's t-tests were applied to the cytokine data analysis. All analyses were performed with 2-tail tests, and the results were considered statistically significant when the *p*-value was less than 0.05.

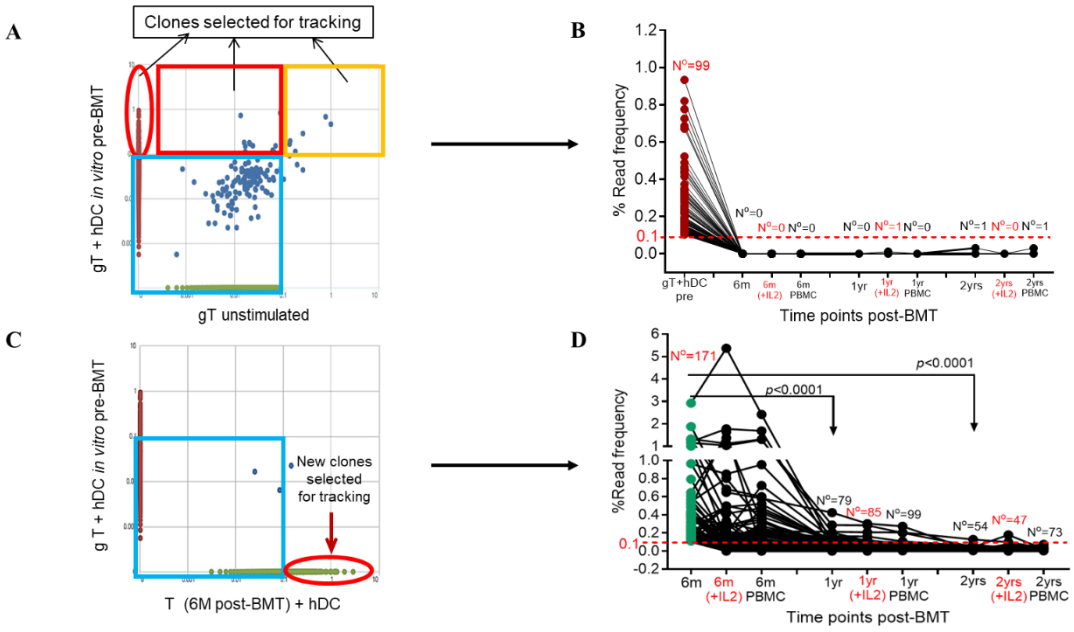

Figure 5. Tracking host-reactive T-cell clones using 'Clonal Tracker™' tool in ImmunoSEQ™ Analyzer Software_v2. A) Identification of host-reactive T-cell clones based on their unique TCRβ CDR3 sequences from pre-BMT bone marrow graft (1E+05 purified T cells) after *in vitro* stimulation with hDCs at 5:1 ratio. Clones with a read frequency ≥ 0.1% (y-axis) compared to unstimulated graft T cells (x-axis) were selected for tracking. **B)** Longitudinal tracking host-reactive T-cell clones (clonal type N°=99) in the patient post-BMT. The y-axis shows % read frequency of each clone type over time (x-axis). Each filled dark red circle represents an individual host-reactive clone type identified amongst graft T cells. Addition of IL-2 to the MLR culture to reverse potential anergy is indicated in red font. **C)** Selection of 'new' alloreactive T-cell clone types (green filled circles) that are ≥ 0.1% frequency and were not identifiable in gT+hDC coculture. **D)** Tracking of these 'new' alloreactive T-cell clones (clonal type N°=171) post-BMT. Numbers at each time point indicate the count of detectable clonal types at any frequency. The Mann-Whitney nonparametric test was used to compare clonal T-cell frequencies. All analyses were performed with 2-tail tests, and the results were considered statistically significant when the *p*-value was less than 0.05.

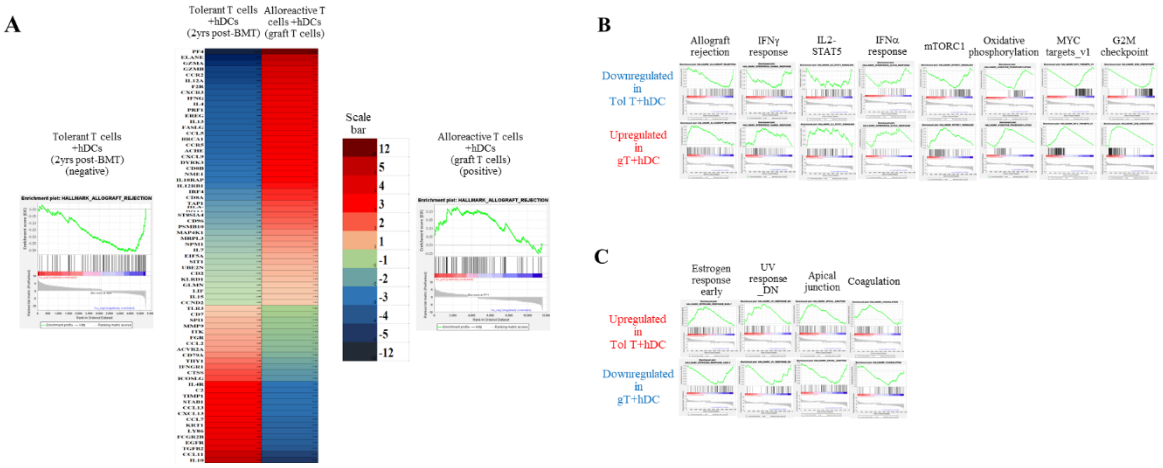

Figure 6. GSEA signaling pathway analysis comparing circulating T cells (donor origin) in tolerant state with T cells from the donor graft. A) After stimulation with hDCs, the 'allograft-rejection' signaling pathway was downregulated in tolerant T cells (Tol T) 2 years post-BMT (left enrichment plot) compared to graft T-cells containing host-reactive clones pre-BMT (right enrichment plot). Individual genes are displayed on a heatmap, with red indicating upregulation (positive rank matric score) and blue indicating downregulation (negative rank matric score). The color scale bar is shown on the right side of the heatmap. **B)** 12 enrichment plots showing pathways that are either downregulated in tolerant T cells (8 plots, first row) compared to graft T cells (second row) after hDC stimulation. **C)** Four enrichment plots showing pathways upregulated in tolerant T cells compared to graft T cells under the same conditions. The genes were selected based on their false discovery rate (FDR) ≤ 0.05 and $\log_2$ fold changes ≥1 or ≤ -1. Data was analyzed using Gene Set Enrichment Analysis®_v4.3.2 (UC San Diego and Broad Institute, Boston MA). Any signaling pathway was considered significantly altered if its nominal p-value ≤0.05' and/or 'FDR q-value of ≤0.25'. For Figures 6A, relative gene expression was visualized through 'conditional formatting' in Microsoft Excel™ (Microsoft Corporation, Inc, Seattle, WA).

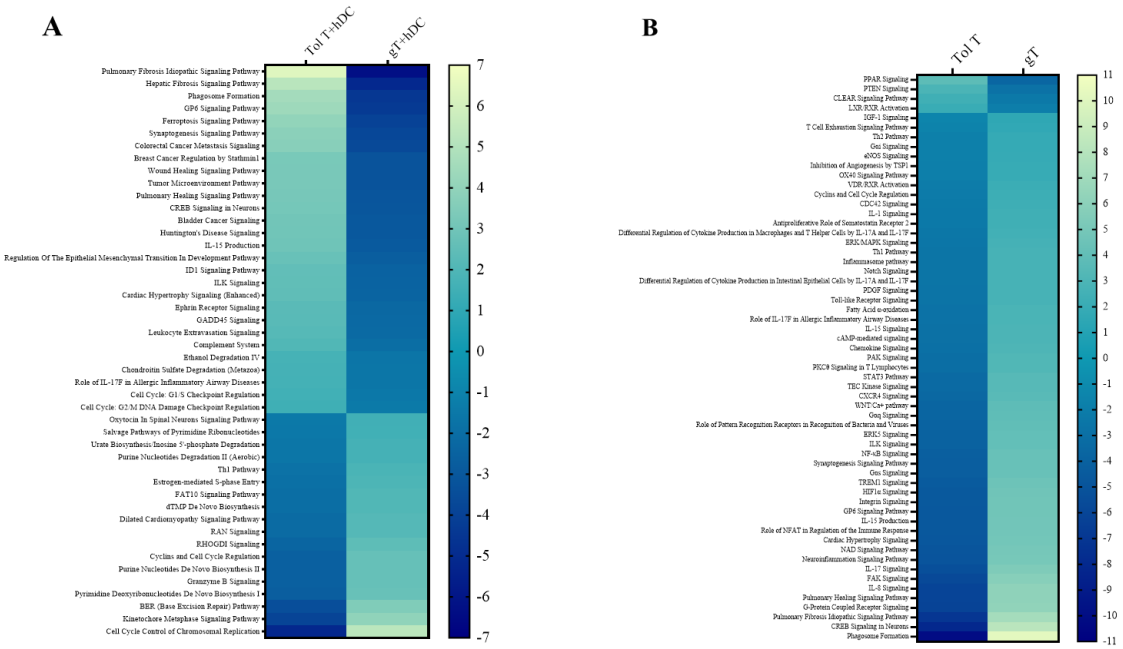

Figure 7. Signaling pathway analysis contrasting circulating T-cells (donor origin) at tolerant state with T cells from the donor graft. A) Ingenuity Pathway Analysis (IPA) comparing tolerant T cells (Tol T, 99.8% donor origin) collected 2 years post-BMT with bone marrow graft T cells (gT) collected pre-BMT, which possessed potential alloreactivity. Both cell populations were stimulated *in vitro* with hDCs for 7 days. **B)** Heatmap comparison of signaling pathways between tolerant T cells (Tol T, left column) and graft T cells (gT, right column) without *in vitro* stimulation. Each box represents a signaling pathway that is either activated (positive z-score, light yellow for most positive) or inhibited (negative z-score, dark blue for most negative). Pathways are listed on the y-axis, and the color scale bar is shown on the right side of the heatmap.

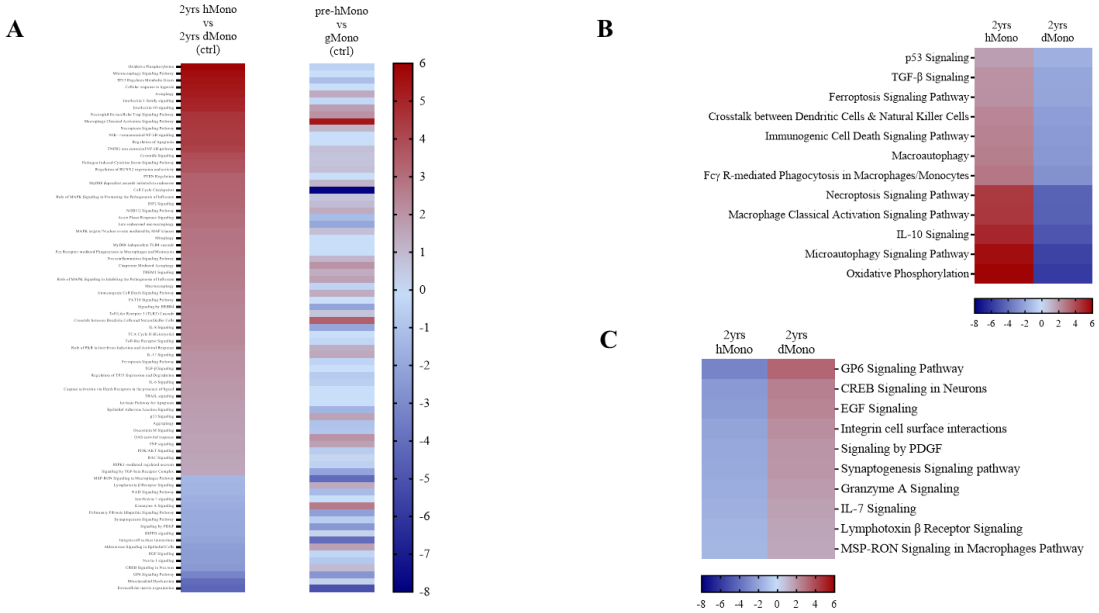

Figure 8: Comparison of signaling pathways between circulating host and donor monocytes from the same time point using IPA software. **A)** Heatmap comparison of signaling pathways between host monocytes (hMono) and donor monocytes (dMono) collected either from flow cytometrically sorted monocytes using unique and HLA-specific antibodies at 2-years post-BMT (left column) or from patient PB and graft pre-BMT (right column). Each box represents a signaling pathway either activated (positive z-score ≥2, dark red as most positive) or inhibited (negative z-score ≤-2, dark blue as most negative). Pathways are listed on the y-axis, and z-score color scale bar is shown on the right side of the heatmap. **B)** Highlighting 12 pathways from left column of panel **A** that are activated in circulating hMono (left column) relative to circulating

dMono (right column). **C)** Highlighting 10 signaling pathways from left column of panel **A** that are quiescent in hMono (left column) compared to dMono (right column).

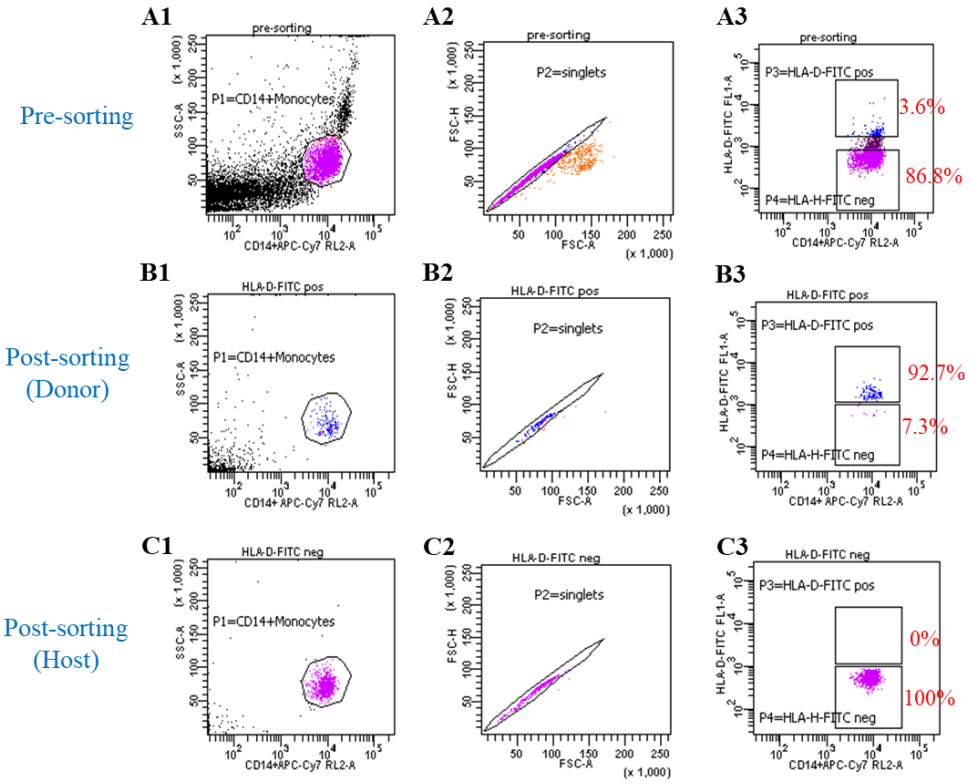

Supplemental Figure 1. Purity of donor and host monocytes from patient PB collected 2 years post-BMT and purified using FACS sorting. A) Gating strategy for donor and host monocytes before sorting, A1, CD14+monocyte selection; A2. singlet selection; A3. Separation of donor and host monocyte based on donor HLA-specific Ab. **B)** Purity of isolated donor monocytes. B1. CD14+monocytes; B2. Singlet selection; B3. purity of isolated donor monocytes after sorting. **C)** Purity of isolated host monocytes. C1. CD14+monocytes; C2. Singlet selection. C3. purity of host monocytes after sorting.

Supplemental Table 1. Patient chimerism post-BMT (% donor)

Chimerism	Post-BOLT/ pre-BMT	1m Post-BMT	2m	3m	6m	9m	1yr	1yr6m	2yrs	3yrs	4yrs	5yrs	6yrs	7yrs6m	9yrs6m
STR[1]															
PB	0	100	72	52	24	21	26	30	28	22	23	17	22	20	21
CD3+T cells	N/A	N/A	27	N/A	94	93	100	95	97	93	92	89	96	96	96
CD33+ Myeloid cells	N/A	100	71	46	17	15	16	14	12	9	9	8	9	8	7
CD19+ B cells											69	62	28	39	38
FC[2] PB															
CD3+T cells	N/A	N/A	8.6	99.2	99.3	99.8	99.8	99.8	99.8	96.6	95.4	98.9	99.8	99.5	99.9
Monocyte (Myeloid)	N/A	N/A	58	40	22	19	17.2	13.5	10.6	13.1	13	7.2	11.3	7.2	6.3
NK cells	N/A	N/A	98	93	58	21	17	14	4.2	6	3.6	3.3	7.3	4	2.2
CD19+ B cells	N/A	N/A	N/A	N/A	N/A	95	94.3	91	86.8	69	81.4	78.7	66.7	61.6	42.6
FC[2] BAL															
CD3+T cells	N/A	N/A	N/A	N/A	99.4	99.4	99.2	97.2	N/A	N/A	N/A	N/A	N/A	N/A	N/A
Monocyte (Myeloid)	N/A	N/A	N/A	N/A	42	34.5	24	24	N/A	N/A	N/A	N/A	N/A	N/A	N/A
NK cells	N/A	N/A	N/A	N/A	93	93	40	36	N/A	N/A	N/A	N/A	N/A	N/A	N/A
CD19+ B cells	N/A	N/A	N/A	N/A	N/A	N/A	63	46	N/A	N/A	N/A	N/A	N/A	N/A	N/A

[1]**Short Tandem Repeat (STR)** testing in the clinical UPMC HLA-laboratory performed on MiniMACS™ purified populations. (There was only 1 test that could be conducted for each assay, and no SD was displayed).
[2]**Flow Cytometry (FC)** in research laboratory. (There was only 1 test that could be conducted for each assay, and no SD was displayed).

Supplemental Table 2. Reconstitution of immune components post-BMT prior to and during thymopoiesis (cell numbers/µL by research FC)

Immune components	Baseline	Post-BLOT/ pre-BMT	1m	2m	3m	6m	9m	1yr	1yr6m	2yrs	3yrs	4yrs	5yrs	6yrs	7yrs6m	9yrs6m
CD3+T cells	74	176	21	2.4	119	406	644	978	955	959	917	859	886	976	655	1334
CD4+T cells	30	25	16	2	98	361	541	753	716	676	628	574	634	646	430	912
CD4+FOXP3+Treg	N/A	2	N/A	N/A	1.5	5	1	6	4.4	22	4.7	8	N/A	25	N/A	N/A
CD4+Tcon[1]	N/A	22	N/A	N/A	90	321	487	642	619	564	596	509	N/A	445	N/A	N/A
CD4+FOXP3+Treg/Tcon	N/A	0.08	N/A	N/A	0.02	0.02	0.002	0.01	0.01	0.04	0.01	0.02	N/A	0.06	N/A	N/A
CD4+T_{EM}[2]	N/A	11	N/A	N/A	16	81	129	192	234	129	82	194	62	N/A	N/A	N/A
CD4+T_{CM}[3]	N/A	14	N/A	N/A	80	250	306	390	152	256	255	188	251	N/A	N/A	N/A
CD4+Tnaive	N/A	0.4	0	0	2	25	88	159	269	276	277	237	222	233	168	374
CD8+T cells	24	98	2	0.4	19	39	86	187	203	249	236	237	213	280	194	386
CD8+T_{EM}[4]	N/A	46	N/A	N/A	7	7	5.4	28	19	14	12.5	29	21	N/A	N/A	N/A
CD8+T_{CM}[5]	N/A	28	N/A	N/A	11	5	11	35	3.4	14	16	5	25	N/A	N/A	N/A
γδT cells	N/A	N/A	N/A	N/A	N/A	3	3	5	6	5	9	11	7	N/A	N/A	N/A
NK T cells	1	0.4	1.4	0	0.1	0.5	2	2	5	5	6.7	7.5	17	6.5	1.3	1.3
NK cells	227	308	173	149	92	208	159	373	215	240	211	173	291	268	211	417
CD19+ B cells	1	34	3	0.5	0.2	4	88	102	177	221	341	232	216	200	160	198
Monocytes	352	259	635	378	253	375	243	342	232	231	146	206	327	205	92	17.4
pDC[6]	6	24	35	7	6	11	7	4	13	7	11.6	8.8	10	9.7	9	7.7
mDC[7]	12	26	64	24	14	20	13	10	23	25	14.6	27	28.8	12	10	22
sjTREC[8]	N/A	369	0	0	0	677	1601	4486	1816	2085	N/A	N/A	N/A	N/A	N/A	N/A
TCRB SCS[9]	N/A	136	48	85	132	170	137	160	159	155	N/A	N/A	N/A	N/A	N/A	N/A

[1]**CD4+ Tcon** = CD4+ conventional T cells (CD3+CD4+CD127+CD25+/-). [2]**CD4+ T_{EM}**=CD4+ effector memory T cells (CD3+CD4+CD45RO+CD62L-).
[3]**CD4+ T_{CM}**=CD4+central memory T cells (CD3+CD4+CD45RO+CD62L+). [4]**CD8+ T_{EM}**=CD8+effector memory T cells (CD3+CD8+CD45RO+CD62L-).
[5]**CD8+ T_{CM}**=CD8+central memory T cells (CD3+CD8+CD45RO+CD62L+). [6]**pDC**=plasmacytoid dendritic cells. [7]**mDC**=myeloid dendritic cells. [8]**sjTREC value** = copies/1E+05 T cells; [9]**TCRB SCS** = TCRβ spectratype complexity score, maximum SCS for 23 of Vβ tested = 184. (There was only 1 test that could be conducted for each assay, and no SD was displayed).

Supplemental Table 3. Potential outcomes and mechanistic interpretation of 'Tolerance' in different MLR setups.

Possible mechanisms	Clonal deletion	Suppression by Treg	Anergy	Suppression by Tr1
In vitro manipulation	**—**	**IL-2 IT***	**IL-2**	**Anti IL-10R Ab**
Proliferation in MLR	**--**	**↑**	**↑**	**↑**
Cytokine Profiling in MLR Supernatant	**--**	**↑ Th1, Th2, Th17**	**↑ Th1, Th2, Th17**	**↑IL-10**
TCR Immunosequencing	**Absent host-reactive clones**	**Representation of host-reactive clones**	**Representation of host-reactive clones**	**Representation of host-reactive clones**

***IL-2-IT** = IL-2-immunotoxin conjugate (Ontak™)

Supplemental Table 4. Clinical chronology and graft characteristics

Characteristics	Pt information
Disease	SCID (IL-7R)
Gender	Female
Age at BMT (years)	14
HLA-match (serological)	2/6
HLA-match (allele level)	1/8
Lung Tx date	9-25-2015
BMT date	1-28-2016
BMT CD34+ N°/kg	5E+06
BMT CD3+ N°/kg	8E+04
DLI date	4-5-2016
DLI CD3 N°/kg	5E+04
Stoppage date of FK506	5-5-2017
GvHD	Grade I, skin
Viral Infection	BKV

Supplemental Table 5. List of genes and their ranks in the downregulated 'Allograft Rejection' pathway analyzed by GSEA software, contrasting tolerant T cells (Tol T) and graft T cells (gT)[1] after *in vitro* stimulation with hDCs.

Row No.	SYMBOL	RANK IN GENE LIST[2]	RANK METRIC SCORE[3]	RUNNING ES[4]	CORE ENRICHMENT[5]
1	IL10	82	5.941	0.0213	No
2	CCL11	200	5.144	0.0308	No
3	TGFB2	482	3.756	0.0001	No
4	EGFR	714	3.286	-0.0239	No
5	FCGR2B	832	3.084	-0.0272	No
6	LY86	912	2.918	-0.0242	No
7	KRT1	954	2.843	-0.0144	No
8	CCL7	1079	2.659	-0.0217	No
9	CXCL13	1498	2.131	-0.0889	No
10	CCL13	1513	2.117	-0.0784	No
11	STAB1	1533	2.097	-0.069	No
12	TIMP1	1541	2.085	-0.0573	No
13	C2	1635	1.99	-0.0628	No
14	IL4R	1781	1.839	-0.0793	No
15	ICOSLG	2161	1.557	-0.1426	No
16	CTSS	2210	1.523	-0.1424	No
17	IFNGR1	2316	1.447	-0.1536	No
18	THY1	2436	1.378	-0.1679	No
19	CD79A	2578	1.288	-0.1871	No
20	ACVR2A	2704	1.212	-0.2036	No
21	CCL2	2737	1.191	-0.2023	No
22	FGR	2777	1.166	-0.2026	No
23	ITK	2840	1.136	-0.2074	No
24	MMP9	2900	1.1	-0.2119	No
25	SPI1	2905	1.098	-0.2058	No
26	CD7	3021	1.039	-0.2215	No
27	TLR3	3053	1.021	-0.2211	No
28	CCND2	3185	-1.036	-0.2399	No
29	IL15	3199	-1.044	-0.2359	No
30	LIF	3218	-1.05	-0.2328	No
31	GLMN	3221	-1.051	-0.2266	No
32	KLRD1	3303	-1.082	-0.2355	No
33	CD2	3360	-1.106	-0.2394	No
34	UBE2N	3364	-1.108	-0.233	No
35	SIT1	3456	-1.139	-0.2435	No
36	EIF5A	3468	-1.146	-0.2384	No
37	IL7	3593	-1.198	-0.2549	No
38	NPM1	3647	-1.227	-0.2574	No
39	MRPL3	3722	-1.258	-0.2638	No
40	MAP4K1	3802	-1.3	-0.271	No
41	PSMB10	3926	-1.38	-0.286	No
42	CD96	3984	-1.417	-0.2882	No
43	ST8SIA4	4051	-1.467	-0.2918	No
44	HLA-DQA1	4082	-1.488	-0.2882	No
45	TAP1	4137	-1.531	-0.2891	No
46	CD8A	4254	-1.63	-0.3013	Yes
47	IRF4	4263	-1.64	-0.2926	Yes
48	IL12RB1	4356	-1.731	-0.2995	Yes
49	IL18RAP	4394	-1.785	-0.2955	Yes
50	NME1	4412	-1.814	-0.2875	Yes
51	CD8B	4461	-1.891	-0.2849	Yes
52	DYRK3	4590	-2.048	-0.2968	Yes
53	CXCL9	4647	-2.132	-0.2943	Yes
54	ACHE	4745	-2.325	-0.2985	Yes
55	CCR5	4784	-2.402	-0.2908	Yes
56	BRCA1	4792	-2.418	-0.277	Yes
57	CCL5	4857	-2.534	-0.2736	Yes
58	FASLG	4860	-2.539	-0.2581	Yes
59	IL13	4918	-2.635	-0.2526	Yes
60	EREG	4919	-2.638	-0.2362	Yes
61	PRF1	4938	-2.689	-0.2229	Yes
62	IL4	4962	-2.743	-0.2102	Yes
63	IFNG	5025	-2.949	-0.2037	Yes
64	CXCR3	5045	-3.015	-0.1886	Yes
65	F2R	5091	-3.217	-0.1771	Yes
66	IL12A	5145	-3.621	-0.1648	Yes
67	CCR2	5163	-3.895	-0.1437	Yes
68	GZMB	5166	-3.953	-0.1194	Yes
69	GZMA	5211	-4.73	-0.0984	Yes
70	ELANE	5227	-5.321	-0.0681	Yes
71	PF4	5258	-11.829	0	Yes

[1]The gT stimulated with hDC was used as a control in the comparison.
[2]**Rank in gene list**: gene rank in gene list based on their differential expression.
[3]**Rank metric score:** the value assigned to each gene in a ranked list, which determines its position within the list and is used to assess how significantly a gene is differentially expressed based on GSEA default metric (signal-to-noise ratio). The higher scores indicate genes that are more significantly differentially expressed (GSEA user guide).
[4]**Running ES**: Running enrichment score that is enrichment score at this point in the ranked list of genes.
[5]**Core enrichment:** genes with a 'Yes' value in this column contribute most to the enrichment result.

Supplemental Table 6. Signaling pathway profiles analyzed by GSEA software comparing tolerant T cells (2 years post-BMT) and graft T cells after *in vitro* stimulation with hDCs.

2yrs Tol T+hDC vs gT+hDC (ctrl) Hallmark pathways	NES[1]	Nom p-value[2]	FDR q-value[3]	Size[4]
Downregulated (15/22 pathways)				
G2M checkpoint	-4.82	0.00E+00	0.00E+00	116
E2F targets	-4.8	0.00E+00	0.00E+00	155
MYC targets_v1	-4.23	0.00E+00	0.00E+00	102
Oxidative phosphorylation	-2.93	0.00E+00	0.00E+00	41
DNA repair	-2.81	0.00E+00	0.00E+00	38
MYC targets_v2	-2.78	0.00E+00	0.00E+00	29
Mitotic spindle	-2.77	0.00E+00	0.00E+00	68
Spermatogenesis	-2.71	0.00E+00	0.00E+00	32
Heme metabolism	-2.31	0.00E+00	1.00E-03	63
mTORC1 signaling	-2.02	0.00E+00	3.00E-03	80
Allograft rejectioon	-1.99	0.00E+00	4.00E-03	71
IFNγ response	-1.53	6.00E-03	6.10E-02	60
Unfolded protein response	-1.52	3.30E-02	6.10E-02	32
IFNα response	-1.33	9.60E-02	1.57E-01	23
IL2/STAT5 signaling	-1.22	1.33E-01	2.48E-01	66
Upregulated (7/22 pathways)				
Epithelial mesenchymal transition	2.68	0.00E+00	0.00E+00	129
Myogenesis	1.83	1.13E-03	2.38E-02	72
UV response_DN	1.81	2.32E-03	2.18E-02	49
Apical junction	1.68	1.12E-03	4.80E-02	68
Estrogen response_early	1.68	1.00E-02	3.91E-02	72
Xenobiotic metabolism	1.56	3.16E-02	9.44E-02	47
Coagulation	1.46	5.04E-02	1.71E-01	57

[1]**NES**: Normalized enrichment score which reflects the degree to which a gene set (or pathway) is concentrated at top (upregulated) or bottom (downregulated) of the ranked list of genes in the expression dataset. Higher NES value (positive or negative) suggests that the gene set is more likely to be associated with observed phenotype (GSEA user guide).
[2]**Nom *p*-value:** Nominal p-value represents statistical significance of a gene set's ES (GSEA user guide).
[3]**FDR q-value** is 'False discovery rate' that is the estimated probability that NES represents a false positive finding. GSEA recommends an FDR threshold of 0.25 or less. A lower q-value indicates a higher confidence in the significance of a gene set (GSEA user guide).
[4]**Size**: number of genes in the gene set after filtering out those genes not in the expression dataset (GSEA user guide).

Supplemental Table 7. Signaling pathway profiles analyzed by IPA software contrasting circulating donor-derived tolerant T cells (Tol T, 2 years post-BMT) and donor bone marrow graft T cells (gT) after *in vitro* stimulation with hDCs.

2yrs Tol T+hDC vs gT+hDC (ctrl)[1] Ingenuity Canonical Pathways	z-score[2]	-log p-value[3]	ratio[4]
Pulmonary Fibrosis Idiopathic Signaling Pathway	6.328	5.3	0.311
Hepatic Fibrosis Signaling Pathway	5.176	2.3	0.258
Phagosome Formation	4.529	2.34	0.247
GP6 Signaling Pathway	4.352	1.4	0.274
Ferroptosis Signaling Pathway	4	2.11	0.299
Synaptogenesis Signaling Pathway	3.771	1.5	0.25
Colorectal Cancer Metastasis Signaling	3.677	1.49	0.254
Breast Cancer Regulation by Stathmin1	3.239	2.72	0.255
Wound Healing Signaling Pathway	3.222	6.11	0.34
Tumor Microenvironment Pathway	3.221	2.44	0.292
Pulmonary Healing Signaling Pathway	3.151	2.73	0.294
*CREB Signaling in Neurons	3.104	0.837	0.224
Bladder Cancer Signaling	3	3.66	0.351
Huntington's Disease Signaling	2.985	1.75	0.259
IL-15 Production	2.92	2.57	0.317
Regulation Of The Epithelial Mesenchymal Transition In Development Pathway	2.711	2	0.318
ID1 Signaling Pathway	2.517	2.41	0.286
ILK Signaling	2.496	3.85	0.318
Cardiac Hypertrophy Signaling (Enhanced)	2.449	1.53	0.24
Ephrin Receptor Signaling	2.263	2.96	0.299
GADD45 Signaling	2.236	1.93	0.339
Leukocyte Extravasation Signaling	2.16	1.37	0.259
Complement System	2	5.4	0.556
Ethanol Degradation IV	1.667	2.1	0.474
Chondroitin Sulfate Degradation (Metazoa)	1.633	1.31	0.429
Role of IL-17F in Allergic Inflammatory Airway Diseases	1.604	1.76	0.348
Cell Cycle: G1/S Checkpoint Regulation	1.528	3.33	0.388
Cell Cycle: G2/M DNA Damage Checkpoint Regulation	1.46	6.74	0.54
Oxytocin In Spinal Neurons Signaling Pathway	-1.508	1.31	0.344
Salvage Pathways of Pyrimidine Ribonucleotides	-1.512	1.55	0.292
Urate Biosynthesis/Inosine 5'-phosphate Degradation	-1.633	1.87	0.5
Purine Nucleotides Degradation II (Aerobic)	-1.633	1.57	0.421
*Th1 Pathway	-1.789	0.442	0.222
Estrogen-mediated S-phase Entry	-1.886	7.91	0.731
FAT10 Signaling Pathway	-2	5.86	0.5
dTMP De Novo Biosynthesis	-2	2.13	0.8
Dilated Cardiomyopathy Signaling Pathway	-2.117	1.65	0.277
RAN Signaling	-2.121	1.89	0.471
RHOGDI Signaling	-2.412	4.3	0.321
Cyclins and Cell Cycle Regulation	-2.646	4.32	0.398
Purine Nucleotides De Novo Biosynthesis II	-2.646	2.64	0.636
Granzyme B Signaling	-2.646	2.08	0.5
Pyrimidine Deoxyribonucleotides De Novo Biosynthesis I	-2.714	2.51	0.478
BER (Base Excision Repair) Pathway	-3.441	3.25	0.432
Kinetochore Metaphase Signaling Pathway	-3.92	13.8	0.542
Cell Cycle Control of Chromosomal Replication	-5.24	11	0.625

[1]Comparison was made of the activation status for signaling pathways between circulating T cells (donor origin) in tolerant state (Tol T) 2-years post-BMT and graft T cells (gT). Both cell types were stimulated with hDC *in vitro*, with graft T cells + hDC serving as a control. The comparison utilized RNAseq gene differential expression data sets generated by CLC Genomics Workbench software and well-established signaling pathways database from IPA software.

[2]**z-score**: IPA software calculates an 'activation z-score' for each pathway, indicating whether the pathway is likely to be activated or inhibited based on the direction of expression changes in the genes involved, as compared with the IPA database. Pathways were selected if their z-score ≥2 or ≤-2.

[3]**-log p-value**: It's a transformed version of p-value that interprets the significance of pathway. IPA uses a default threshold of -log p-value ≥1.3. The higher value holds greater significance.

[4]**Ratio**: proportion of presented dataset genes in the total number of genes in that pathway within the IPA reference set.

*These 2 pathways had z-score ≥2 or ≤-2 after hDC stimulation even though their -log p-value <1.3.

Supplemental Table 8. Signaling pathway profiles analyzed by IPA software contrasting tolerant T cells (Tol T, 2 years post-BMT) and bone marrow graft T cells (gT) without any *in vitro* stimulation.

2yrs Tol T vs gT (ctrl)[1] Ingenuity Canonical Pathways	z-score[2]	-log p-value[3]	Ratio[4]	2yrs Tol T vs gT (ctrl)[1] Ingenuity Canonical Pathways	z-score[2]	-log p-value[3]	Ratio[4]
RHOGDI Signaling	3.922	3.24	0.226	PKC0 Signaling in T Lymphocytes	-3.138	1.52	0.178
PPAR Signaling	3.71	1.48	0.212	Osteoarthritis Pathway	-3.159	10.9	0.315
Antioxidant Action of Vitamin C	3.638	1.86	0.224	Putrescine Degradation III	-3.162	4.62	0.588
PTEN Signaling	2.858	3.37	0.247	Tryptophan Degradation X (Mammalian, via Tryptamine)	-3.162	4.06	0.526
CLEAR Signaling Pathway	2.335	1.94	0.192	Oxidative Ethanol Degradation III	-3.162	2.31	0.345
Extrinsic Prothrombin Activation Pathway	2.236	1.74	0.375	Oxytocin In Spinal Neurons Signaling Pathway	-3.162	1.97	0.312
LXR/RXR Activation	1.976	4.15	0.276	Phospholipases	-3.207	1.96	0.258
IGF-1 Signaling	-1.508	1.48	0.212	Sphingosine-1-phosphate Signaling	-3.266	3.49	0.265
Apelin Adipocyte Signaling Pathway	-1.604	1.26	0.209	Thrombin Signaling	-3.266	1.97	0.2
T Cell Exhaustion Signaling Pathway	-1.606	1.5	0.178	Production of Nitric Oxide and Reactive Oxygen Species in Macrophages	-3.286	1.45	0.191
Aryl Hydrocarbon Receptor Signaling	-1.789	3.55	0.252				
Th2 Pathway	-1.8	7.11	0.323	Ethanol Degradation II	-3.317	3.18	0.407
Gαi Signaling	-1.8	3.02	0.243	FcγRIIB Signaling in B Lymphocytes	-3.317	1.67	0.229
eNOS Signaling	-1.826	2.66	0.23	Dermatan Sulfate Biosynthesis (Late Stages)	-3.317	1.54	0.262
Inhibition of Angiogenesis by TSP1	-1.89	3.04	0.375	Ephrin B Signaling	-3.357	2.34	0.264
OX40 Signaling Pathway	-1.89	1.6	0.189	Relaxin Signaling	-3.357	1.69	0.205
Neuregulin Signaling	-1.941	2.3	0.235	Ephrin Receptor Signaling	-3.411	3.52	0.234
Salvage Pathways of Pyrimidine Deoxyribonucleotides	-2	1.55	0.444	STAT3 Pathway	-3.43	7.87	0.333
Prostanoid Biosynthesis	-2	1.38	0.4	TEC Kinase Signaling	-3.43	5	0.224
Oleate Biosynthesis II (Animals)	-2	1.38	0.4	Ethanol Degradation IV	-3.464	5.91	0.632
Pentose Phosphate Pathway	-2	1.38	0.4	Noradrenaline and Adrenaline Degradation	-3.464	3.34	0.4
Corticotropin Releasing Hormone Signaling	-2.041	1.41	0.197	Serotonin Degradation	-3.5	2.33	0.281
VDR/RXR Activation	-2.111	2.01	0.247	B Cell Receptor Signaling	-3.528	26.9	0.368
Actin Nucleation by ARP-WASP Complex	-2.121	2.45	0.253	CXCR4 Signaling	-3.53	2.79	0.229
Regulation of Actin-based Motility by Rho	-2.138	2.91	0.255	PI3K Signaling in B Lymphocytes	-3.53	1.79	0.212
Mitotic Roles of Polo-Like Kinase	-2.138	2.25	0.27	MSP-RON Signaling In Cancer Cells Pathway	-3.53	1.28	0.194
Natural Killer Cell Signaling	-2.16	2.57	0.218	Sperm Motility	-3.545	8.57	0.287
Cyclins and Cell Cycle Regulation	-2.183	1.39	0.217	Dopamine Degradation	-3.606	5.31	0.542
Epithelial Adherens Junction Signaling	-2.197	2.51	0.226	Actin Cytoskeleton Signaling	-3.651	3.77	0.229
CDC42 Signaling	-2.236	3.25	0.208	Cell Cycle Control of Chromosomal Replication	-3.742	1.66	0.25
Remodeling of Epithelial Adherens Junctions	-2.236	2.81	0.288	WNT/Ca+ pathway	-3.771	2.89	0.292
Eicosanoid Signaling	-2.236	2.11	0.262	Pancreatic Adenocarcinoma Signaling	-3.771	1.61	0.21
Phenylalanine Degradation IV (Mammalian, via Side Chain)	-2.236	1.42	0.357	Leukocyte Extravasation Signaling	-3.795	4.2	0.249
Gα12/13 Signaling	-2.268	1.96	0.218	Gαq Signaling	-3.8	1.61	0.2
Estrogen-mediated S-phase Entry	-2.333	2.14	0.346	Systemic Lupus Erythematosus In T Cell Signaling Pathway	-3.812	1.65	0.178
IL-1 Signaling	-2.333	1.58	0.219	Role of Pattern Recognition Receptors in Recognition of Bacteria and Viruses	-3.9	5.06	0.281
Antiproliferative Role of Somatostatin Receptor 2	-2.333	1.28	0.216				
Tryptophan Degradation to 2-amino-3-carboxymuconate Semialdehyde	-2.449	5.09	1	GNRH Signaling	-3.962	1.25	0.185
				ERK5 Signaling	-4	1.86	0.243
Choline Biosynthesis III	-2.449	2.06	0.429	ILK Signaling	-4.004	2.73	0.221
Differential Regulation of Cytokine Production in Macrophages and T Helper Cells by IL-17A and IL-17F	-2.449	1.49	0.333	Regulation Of The Epithelial Mesenchymal Transition By Growth Factors Pathway	-4.012	3.14	0.229
Regulation Of The Epithelial Mesenchymal Transition In Development Pathway	-2.524	2.17	0.247	Factors Promoting Cardiogenesis in Vertebrates	-4.017	2.31	0.223
Cardiac β-adrenergic Signaling	-2.524	2.08	0.21	Fcγ Receptor-mediated Phagocytosis in Macrophages and Monocytes	-4.025	1.46	0.215
ERK/MAPK Signaling	-2.556	2.6	0.214				
RHOA Signaling	-2.6	1.95	0.221	Cholecystokinin/Gastrin-mediated Signaling	-4.025	1.42	0.205
Th1 Pathway	-2.646	5.95	0.316	HMGB1 Signaling	-4.041	3.78	0.252
Role of IL-17A in Psoriasis	-2.646	2.81	0.5	Systemic Lupus Erythematosus In B Cell Signaling Pathway	-4.093	31	0.36
Inflammasome pathway	-2.646	1.79	0.35	Xenobiotic Metabolism AHR Signaling Pathway	-4.146	2.57	0.266
Role of NANOG in Mammalian Embryonic Stem Cell Pluripotency	-2.646	1.62	0.212	Endothelin-1 Signaling	-4.226	1.71	0.199
				NF-κB Signaling	-4.23	3.44	0.207
Notch Signaling	-2.646	1.53	0.27	Synaptogenesis Signaling Pathway	-4.243	1.45	0.179
Differential Regulation of Cytokine Production in Intestinal Epithelial Cells by IL-17A and IL-17F	-2.646	1.45	0.304	Gαs Signaling	-4.264	3.02	0.25
				ID1 Signaling Pathway	-4.45	6.31	0.276
RAC Signaling	-2.668	2.3	0.226	TREM1 Signaling	-4.49	8.61	0.431
PDGF Signaling	-2.668	1.26	0.209	HIF1α Signaling	-4.621	3.09	0.225
Paxillin Signaling	-2.673	2.51	0.245	Phospholipase C Signaling	-4.629	5.61	0.22
Toll-like Receptor Signaling	-2.673	2.01	0.247	Neurovascular Coupling Signaling Pathway	-4.629	1.81	0.197
HGF Signaling	-2.683	4.3	0.275	Adrenomedullin signaling pathway	-4.644	2.53	0.216
Nitric Oxide Signaling in the Cardiovascular System	-2.683	1.31	0.202	Glioblastoma Multiforme Signaling	-4.667	4.9	0.268
Macropinocytosis Signaling	-2.714	4.56	0.329	Integrin Signaling	-4.667	2.31	0.21
NAD biosynthesis II (from tryptophan)	-2.828	4.75	0.727	Role of Hypercytokinemia/hyperchemokinemia in the Pathogenesis of Influenza	-4.69	2.87	0.275
Fatty Acid α-oxidation	-2.828	3.15	0.5				
Role of IL-17F in Allergic Inflammatory Airway Diseases	-2.828	1.62	0.261	GP6 Signaling Pathway	-4.707	2.7	0.242
Basal Cell Carcinoma Signaling	-2.84	2.12	0.257	White Adipose Tissue Browning Pathway	-4.707	1.56	0.204
Glioma Signaling	-2.84	1.46	0.205	IL-15 Production	-4.727	8.63	0.358
Gustation Pathway	-2.874	1.28	0.185	Role of NFAT in Regulation of the Immune Response	-4.727	3.97	0.212
IL-15 Signaling	-2.887	29.1	0.426	Cardiac Hypertrophy Signaling	-4.768	1.81	0.192
cAMP-mediated signaling	-2.887	4.23	0.238	Signaling by Rho Family GTPases	-4.841	5.03	0.242
Chondroitin Sulfate Biosynthesis (Late Stages)	-2.887	1.7	0.267	NAD Signaling Pathway	-4.914	1.28	0.193
Apelin Endothelial Signaling Pathway	-2.982	1.67	0.207	Neuroinflammation Signaling Pathway	-4.993	5.67	0.241
Histamine Degradation	-3	5.02	0.692	Wound Healing Signaling Pathway	-5.345	4.15	0.235
Tryptophan Degradation III (Eukaryotic)	-3	3.18	0.407	IL-17 Signaling	-5.376	2.69	0.223
Glioma Invasiveness Signaling	-3	2.8	0.282	Xenobiotic Metabolism PXR Signaling Pathway	-5.667	1.86	0.205
PCP (Planar Cell Polarity) Pathway	-3	2.49	0.283	FAK Signaling	-5.762	7.55	0.21
Glutathione-mediated Detoxification	-3	2.02	0.333	IL-8 Signaling	-6.112	5.44	0.262
14-3-3-mediated Signaling	-3	1.53	0.206	Pulmonary Healing Signaling Pathway	-6.147	6.85	0.284
Chemokine Signaling	-3	1.4	0.221	Colorectal Cancer Metastasis Signaling	-6.181	6.7	0.261
Ovarian Cancer Signaling	-3.051	2.46	0.224	Hepatic Fibrosis Signaling Pathway	-6.188	7.77	0.244
Dermatan Sulfate Biosynthesis	-3.051	1.39	0.236	G-Protein Coupled Receptor Signaling	-6.237	4.93	0.2
Pyroptosis Signaling Pathway	-3.128	2.52	0.256	Tumor Microenvironment Pathway	-6.272	4.91	0.264
Endocannabinoid Neuronal Synapse Pathway	-3.128	1.81	0.209	Dendritic Cell Maturation	-6.425	7.79	0.249
PAK Signaling	-3.13	4.24	0.282	Breast Cancer Regulation by Stathmin1	-6.755	5.54	0.211
P2Y Purigenic Receptor Signaling Pathway	-3.13	1.76	0.212	Pulmonary Fibrosis Idiopathic Signaling Pathway	-7.18	6.34	0.245
Crosstalk between Dendritic Cells and Natural Killer Cells	-3.138	5.36	0.33	Cardiac Hypertrophy Signaling (Enhanced)	-7.298	6.61	0.223
Kinetochore Metaphase Signaling Pathway	-3.138	4.68	0.299	CREB Signaling in Neurons	-8.171	6.01	0.213
				Phagosome Formation	-10.171	15.1	0.257

[1]Comparison was made of the activation status for signaling pathways between circulating T cells (donor origin) in tolerant state (Tol T) 2-years post-BMT and graft T cells (gT), without hDC *in vitro* stimulation. Graft T cells served as a control. The comparison utilized RNAseq gene differential expression data sets generated by CLC Genomics Workbench software and well-established signaling pathways database from IPA software.

[2]**z-score**: IPA software calculates an 'activation z-score' for each pathway, indicating whether the pathway is likely to be activated or inhibited based on the direction of expression changes in the genes involved, as compared with the IPA. Pathways were selected if their z-score ≥2 or ≤-2.

[3]**-log p-value**: It's a transformed version of p-value that interprets the significance of pathway. IPA uses a default threshold of -log p-value ≥1.3. The higher value holds greater significance.

[4]**Ratio**: proportion of presented dataset genes in the total number of genes in that pathway within the IPA reference set.

Supplemental Table 9. Signaling pathway profiles analyzed by IPA software contrasting co-existing circulating host and donor monocytes at 2 years post-BMT.

2yrs hMono vs 2yrs dMono (ctrl)[1] Ingenuity Canonical Pathways	z-score[2]	-log p-value[3]	Ratio[4]
Neutrophil degranulation	11.415	39.7	0.54
SRP-dependent cotranslational protein targeting to membrane	8.102	29.9	0.772
Eukaryotic Translation Initiation	7.398	25.3	0.713
Eukaryotic Translation Elongation	7.171	21.9	0.737
Selenoamino acid metabolism	7.14	19.6	0.682
Eukaryotic Translation Termination	7.034	20.5	0.723
Response of EIF2AK4 (GCN2) to amino acid deficiency	6.905	21.1	0.709
Nonsense-Mediated Decay (NMD)	6.333	22.3	0.692
Oxidative Phosphorylation	5.899	18	0.664
Microautophagy Signaling Pathway	5.612	7.48	0.459
TP53 Regulates Metabolic Genes	5.461	9.88	0.58
Cellular response to hypoxia	5.376	6.54	0.533
Electron transport, ATP synthesis, and heat production by uncoupling proteins	5.237	20.7	0.656
Autophagy	5.222	5.38	0.397
Class I MHC mediated antigen processing and presentation	5.157	10.4	0.411
Interleukin-1 family signaling	5.077	6.21	0.457
Cachexia Signaling Pathway	5.058	4.74	0.356
Major pathway of rRNA processing in the nucleolus and cytosol	5.051	14.6	0.527
Neddylation	5.027	5.4	0.388
Interleukin-10 signaling	4.95	9.67	0.711
Degradation of beta-catenin by the destruction complex	4.824	8.05	0.538
Mitotic Metaphase and Anaphase	4.796	5.45	0.391
Antigen Presentation Pathway	4.796	5.24	0.605
Regulation of mitotic cell cycle	4.743	4.35	0.455
Mitochondrial protein import	4.596	4.6	0.5
Neutrophil Extracellular Trap Signaling Pathway	4.585	11.5	0.418
Macrophage Classical Activation Signaling Pathway	4.5	3.16	0.367
Iron uptake and transport	4.491	2.2	0.414
Hedgehog ligand biogenesis	4.459	5.41	0.523
Necroptosis Signaling Pathway	4.45	2.52	0.359
KEAP1-NFE2L2 pathway	4.427	3.95	0.44
Regulation of Apoptosis	4.352	7.69	0.623
NIK-->noncanonical NF-kB signaling	4.352	5.91	0.55
CGAS-STING Signaling Pathway	4.341	2.99	0.381
Sphingolipid metabolism	4.243	1.85	0.368
Synthesis of DNA	4.23	3.2	0.395
TNFR2 non-canonical NF-kB pathway	4.218	6.95	0.559
Protein Sorting Signaling Pathway	4.007	5.08	0.407
COPII-mediated vesicle transport	4.004	3.78	0.458
C-type lectin receptors (CLRs)	3.906	11.8	0.531
RAB geranylgeranylation	3.9	3.16	0.446
Ceramide Signaling	3.893	5.15	0.473
Metabolism of polyamines	3.889	5.57	0.542
DNA Replication Pre-Initiation	3.833	4.53	0.442
Hedgehog 'on' state	3.812	5.97	0.5
Response to elevated platelet cytosolic Ca2+	3.81	4.05	0.409
Hepatic Cholestasis	3.787	1.44	0.313
ISG15 antiviral mechanism	3.78	2.13	0.394
Detoxification of Reactive Oxygen Species	3.771	2.66	0.486
Pathogen Induced Cytokine Storm Signaling Pathway	3.714	3.54	0.341
MyD88:MAL(TIRAP) cascade initiated on plasma membrane	3.71	3.22	0.5
Peroxisomal protein import	3.674	1.7	0.381
Regulation of RUNX2 expression and activity	3.667	4.93	0.493
Signaling by NOTCH4	3.647	8.93	0.573
NAFLD Signaling Pathway	3.622	4.55	0.382
Transcriptional regulation by RUNX3	3.507	6.12	0.49
Cargo concentration in the ER	3.5	2.24	0.471
MHC class II antigen presentation	3.464	2.86	0.381
Mitochondrial translation	3.452	2.43	0.385
E3 ubiquitin ligases ubiquitinate target proteins	3.413	5.9	0.564
RHO GTPases Activate WASPs and WAVEs	3.411	5.13	0.611
Protein ubiquitination	3.357	2.45	0.5
Fc epsilon receptor (FCERI) signaling	3.347	3.89	0.374
ABC-family proteins mediated transport	3.328	7.62	0.515
PTEN Regulation	3.328	7.27	0.46
MyD88 dependent cascade initiated on endosome	3.3	3.89	0.581
Regulation of mRNA stability by proteins that bind AU-rich elements	3.3	1.72	0.409
Cell Cycle Checkpoints	3.266	3.61	0.353
Role of MAPK Signaling in Promoting the Pathogenesis of Influenza	3.244	2.33	0.373
EIF2 Signaling	3.204	25.2	0.595
S Phase	3.202	3.93	0.43
NRF2-mediated Oxidative Stress Response	3.162	4	0.374
Cristae formation	3.153	3.3	0.548
Endosomal Sorting Complex Required For Transport (ESCRT)	3.153	3.3	0.548
NOD1/2 Signaling Pathway	3.098	2.32	0.347
Cytoprotection by HMOX1	3.053	4.48	0.5
Actin Nucleation by ARP-WASP Complex	3.053	4.33	0.451
MyD88 cascade initiated on plasma membrane	3.051	2.37	0.52
Mitotic G1 phase and G1/S transition	3	6.74	0.466
Differential Regulation of Cytokine Production in Macrophages and T Helper Cells by IL-17A and IL-17F	3	1.64	0.5
Protein Ubiquitination Pathway	2.997	9.3	0.429
Acute Phase Response Signaling	2.994	4.41	0.391
Late endosomal microautophagy	2.982	3.77	0.559
Signaling by ROBO receptors	2.941	4.86	0.44
The citric acid (TCA) cycle and respiratory electron transport	2.921	5.33	0.545
Agrin Interactions at Neuromuscular Junction	2.887	3.54	0.456
Apelin Adipocyte Signaling Pathway	2.887	1.44	0.349
HMGB1 Signaling	2.885	4.73	0.409
TCR signaling	2.869	12.1	0.556
RAS processing	2.84	3.82	0.625
Mitophagy	2.84	2.45	0.5
Signaling by CSF3 (G-CSF)	2.84	2.45	0.5
MAPK targets/ Nuclear events mediated by MAP kinases	2.84	1.97	0.455
MyD88-independent TLR4 cascade	2.837	4.24	0.568
Signaling by Insulin receptor	2.828	1.83	0.419
Fcγ Receptor-mediated Phagocytosis in Macrophages and Monocytes	2.795	2.71	0.398
Transcriptional regulation by RUNX1	2.794	4.51	0.408
Cargo recognition for clathrin-mediated endocytosis	2.777	3.06	0.4
Signaling by the B Cell Receptor (BCR)	2.734	2.94	0.365
Neuroinflammation Signaling Pathway	2.714	4.8	0.365
Glutathione Redox Reactions I	2.714	2.05	0.5
CDP-diacylglycerol Biosynthesis I	2.714	1.58	0.444
Chaperone Mediated Autophagy	2.673	3.71	0.636
Remodeling of Epithelial Adherens Junctions	2.673	2.32	0.409
TREM1 Signaling	2.667	5.1	0.5
Alpha-protein kinase 1 signaling pathway	2.646	2.06	0.636
Pexophagy	2.646	2.06	0.636
Amyloid fiber formation	2.646	1.94	0.384
RAF/MAP kinase cascade	2.626	5.3	0.382
Role of MAPK Signaling in Inhibiting the Pathogenesis of Influenza	2.6	1.44	0.355
Protein folding	2.592	4.18	0.439
Deubiquitination	2.574	5.75	0.388
Folate Signaling Pathway	2.558	1.76	0.393
Macroautophagy	2.556	3.56	0.462
Regulation of Actin-based Motility by Rho	2.535	3.17	0.4
Glycerophospholipid biosynthesis	2.535	1.69	0.354
Superpathway of Cholesterol Biosynthesis	2.5	4.03	0.607
Signaling by FGFR3	2.5	1.48	0.4
Cholesterol biosynthesis	2.496	2.37	0.52
Multiple Sclerosis Signaling Pathway	2.492	2.3	0.338
Mitotic Prophase	2.48	5.05	0.456
Immunogenic Cell Death Signaling Pathway	2.475	2.1	0.381
COPI-mediated anterograde transport	2.469	3.47	0.416
Nucleotide Excision Repair	2.466	2.43	0.385
FAT10 Signaling Pathway	2.449	5.9	0.564
Ephrin Receptor Signaling	2.449	3.06	0.358
Endocannabinoid Cancer Inhibition Pathway	2.449	3.05	0.377
NLR signaling pathways	2.449	2.43	0.429
Pentose Phosphate Pathway	2.449	1.65	0.6
Signaling by ERBB4	2.4	1.87	0.397
Toll Like Receptor 3 (TLR3) Cascade	2.357	3.65	0.562
Crosstalk between Dendritic Cells and Natural Killer Cells	2.353	1.79	0.363
Signaling by NTRK1 (TRKA)	2.335	2.08	0.383
Advanced glycosylation endproduct receptor signaling	2.333	2.92	0.692
Vitamin-C Transport	2.333	1.32	0.435
IL-8 Signaling	2.321	3.89	0.374
Insertion of tail-anchored proteins into the endoplasmic reticulum membrane	2.309	2.44	0.545
TCA Cycle II (Eukaryotic)	2.309	2.44	0.545
Phosphatidylglycerol Biosynthesis II (Non-plastidic)	2.309	1.71	0.448
Energy dependent regulation of mTOR by LKB1-AMPK	2.309	1.33	0.414
TAK1-dependent IKK and NF-kappa-B activation	2.294	3.85	0.523
Toll-like Receptor Signaling	2.294	3.49	0.442
Senescence-Associated Secretory Phenotype (SASP)	2.268	1.94	0.384
MAP kinase activation	2.236	3.27	0.513
Role of PKR in Interferon Induction and Antiviral Response	2.188	3.45	0.394
Cholesterol Biosynthesis I	2.121	2.17	0.615
Cholesterol Biosynthesis II (via 24,25-dihydrolanosterol)	2.121	2.17	0.615
Cholesterol Biosynthesis III (via Desmosterol)	2.121	2.17	0.615
Gene Silencing by RNA	2.121	1.3	0.337
Amino acids regulate mTORC1	2.117	3.81	0.491
Interconversion of nucleotide di- and triphosphates	2.111	1.91	0.5
IL-17 Signaling	2.066	1.95	0.335
Ferroptosis Signaling Pathway	2.064	2.52	0.37
Mitotic G2-G2/M phases	2.063	10.4	0.472
Regulation of lipid metabolism by PPARalpha	2.058	1.31	0.328
TGF-β Signaling	2.043	1.39	0.34
Clathrin-mediated endocytosis	2.023	4.72	0.426
MTOR signalling	2	3.4	0.571
Glutathione Redox Reactions II	2	2.36	1
Regulation of TP53 Expression and Degradation	2	1.59	0.41
Zymosterol Biosynthesis	2	1.39	0.667
fMLP Signaling in Neutrophils	1.98	7.47	0.481
XBP1(S) activates chaperone genes	1.964	2.31	0.438
Induction of Apoptosis by HIV1	1.961	2.66	0.429
Cellular response to heat stress	1.961	2.08	0.371
Th1 Pathway	1.953	8.6	0.513
Gluconeogenesis I	1.941	2.37	0.52
Thrombin signalling through proteinase activated receptors (PARs)	1.941	1.34	0.406
RAB GEFs exchange GTP for GDP on RABs	1.915	1.95	0.371
IL-6 Signaling	1.905	5.44	0.442
Caspase activation via Death Receptors in the presence of ligand	1.897	2.69	0.625
Valine Degradation I	1.897	2.31	0.55
TRAIL signaling	1.89	3.34	0.875
CSDE1 Signaling Pathway	1.877	2.94	0.455
TCF dependent signaling in response to WNT	1.812	4.75	0.392
Transcriptional Regulation by YY1X	1.807	1.83	0.425
Intrinsic Pathway for Apoptosis	1.8	2.94	0.455
Angiopoietin Signaling	1.789	2.25	0.395
RHOA Signaling	1.769	3.51	0.402
EPH-Ephrin signaling	1.761	3.47	0.424
Cholecystokinin/Gastrin-mediated Signaling	1.761	2.54	0.376
Epithelial Adherens Junction Signaling	1.756	8.31	0.471
Role of p14/p19ARF in Tumor Suppression	1.732	1.33	0.414
p53 Signaling	1.706	1.76	0.357
Oncostatin M Signaling	1.698	2.2	0.442
Aggrephagy	1.698	1.5	0.395
Circadian Clock	1.698	1.31	0.362
Apelin Endothelial Signaling Pathway	1.677	3.1	0.381
OAS antiviral response	1.633	1.94	0.667
Pathogenesis of Multiple Sclerosis	1.633	1.94	0.667
TNF signaling	1.616	5.45	0.544
TBC/RABGAPs	1.606	2.07	0.432
UVC-Induced MAPK Signaling	1.606	1.96	0.412
PI3K/AKT Signaling	1.605	4.84	0.394
Transcriptional Regulation by NPAS4	1.604	1.35	0.4
Translocation of SLC2A4 (GLUT4) to the plasma membrane	1.569	1.57	0.366
RAC Signaling	1.54	5.91	0.445
Sertoli Cell-Germ Cell Junction Signaling Pathway (Enhanced)	1.539	6.54	0.408
MicroRNA Biogenesis Signaling Pathway	1.522	4.79	0.399
IL-17A Signaling in Gastric Cells	1.508	2.18	0.5
Dopamine Degradation	1.508	1.59	0.458
Glycolysis I	1.508	1.59	0.458
RIPK1-mediated regulated necrosis	1.5	2.58	0.5
Wound Healing Signaling Pathway	1.463	2.26	0.332
Signaling by TGF-beta Receptor Complex	1.46	2.43	0.434
MSP-RON Signaling in Macrophages Pathway	-1.474	3.19	0.397
Glioblastoma Multiforme Signaling	-1.511	3.34	0.375
Breast Cancer Regulation by Stathmin1	-1.516	2.59	0.308
Lymphotoxin β Receptor Signaling	-1.528	2.68	0.444
NAD Signaling Pathway	-1.543	1.57	0.331
HER-2 Signaling in Breast Cancer	-1.565	6	0.404
Ribonucleotide Reductase Signaling Pathway	-1.576	2.49	0.353
ATM Signaling	-1.667	4.81	0.455
Interleukin-7 signaling	-1.667	1.61	0.476
BBSome Signaling Pathway	-1.69	2	0.304
Erythropoietin Signaling Pathway	-1.692	2.4	0.351
RUNX1 regulates megakaryocyte differentiation and platelet function	-1.698	2.55	0.431
G alpha (12/13) signalling events	-1.768	2.47	0.4
Huntington's Disease Signaling	-1.769	7.15	0.401
Orexin Signaling Pathway	-1.789	2.78	0.345
Granzyme A Signaling	-1.808	5.78	0.521
Parkinson's Signaling Pathway	-1.857	6.9	0.395
Formation of WDR5-containing histone-modifying complexes	-1.886	1.95	0.429
Signaling by SCF-KIT	-1.886	1.83	0.419
Pulmonary Fibrosis Idiopathic Signaling Pathway	-1.91	2.07	0.317
Synaptogenesis Signaling Pathway	-1.925	5.13	0.369
ROBO SLIT Signaling Pathway	-1.941	4.26	0.419
HIPPO signaling	-1.964	2.49	0.395
Signaling by PDGF	-1.964	1.31	0.362
Integrin cell surface interactions	-2.121	2.01	0.376
Spliceosomal Cycle	-2.132	2.43	0.434
Small Cell Lung Cancer Signaling	-2.132	1.58	0.351
Aldosterone Signaling in Epithelial Cells	-2.335	3.09	0.369
Netrin-1 signaling	-2.4	2.07	0.42
Sensory processing of sound by outer hair cells of the cochlea	-2.4	1.56	0.382
EGF Signaling	-2.4	1.47	0.375
CREB Signaling in Neurons	-2.514	2.12	0.301
Adrenergic Receptor Signaling Pathway (Enhanced)	-2.54	1.59	0.321
Sensory processing of sound by inner hair cells of the cochlea	-2.6	1.47	0.362
Cilium Assembly	-2.65	8.51	0.446
NCAM signaling for neurite out-growth	-2.711	1.6	0.377
Histone Modification Signaling Pathway	-2.714	3.07	0.34
Neuropathic Pain Signaling in Dorsal Horn Neurons	-2.744	1.41	0.34
GP6 Signaling Pathway	-3.244	1.46	0.333
RHO GTPase cycle	-3.298	10.3	0.396
Coronavirus Pathogenesis Pathway	-3.313	7.56	0.438
Docosahexaenoic Acid (DHA) Signaling	-3.534	2.48	0.336
Neurexins and neuroligins	-3.71	1.39	0.368
Acetylcholine Receptor Signaling Pathway	-3.81	1.73	0.326
Mitochondrial Dysfunction	-4.11	14.7	0.456
Extracellular matrix organization	-4.333	1.46	0.34

[1]A comparison of the activation status of signaling pathways between host-monocytes (hMono) and donor monocytes (dMono) at tolerant stage 2-years post-BMT. The dMono was used as a control in comparison. The comparison was based on their RNAseq gene differential expression data sets generated by CLC Genomic Workbench software and the database of well-established signaling pathways from IPA software.

[2]**z-score**: IPA software calculates an 'activation z-score' for each pathway, indicating whether the pathway is likely to be activated or inhibited based on the direction of expression changes in the genes involved, as compared with the IPA database. Pathways were selected if their z-score ≥2 or ≤-2.

[3]**-log p-value**: It's a transformed version of p-value that interprets the significance of pathway. IPA uses a default threshold of -log p-value ≥1.3. The higher value holds greater significance.

[4]**Ratio**: proportion of presented dataset genes in the total number of genes in that pathway within the IPA reference set.